공학박사 학위논문

Deep Learning-Based Blood Pressure Prediction

딥러닝 기반 혈압 예측 기법

2020년 8월

서울대학교 대학원

전기·정보 공학부

백 상 현

Deep Learning-Based Blood Pressure Prediction

지도교수 윤 성 로

이 논문을 공학박사 학위논문으로 제출함

2020년 8월

서울대학교 대학원

전기·정보 공학부

백 상 현

백상현의 박사 학위논문을 인준함

2020년 8월

위 원 장 _____ (인)

부위원장 _____ (인)

위 원 _____ (인)

위 원 _____ (인)

위 원 _____ (인)

Abstract

While COVID-19 is changing the world's social profile, it is expected that the telemedicine sector, which has not been activated due to low regulation and reliability, will also undergo a major change. As COVID-19 spreads in the United States, the US Department of Health & Human Services temporarily loosens the standards for telemedicine, while enabling telemedicine using Facebook, Facebook Messenger-based video chat, Hangouts, and Skype. The expansion of the telemedicine market is expected to quickly transform the existing treatment-oriented hospital-led medical market into a digital healthcare service market focused on prevention and management through wearables, big data, and health records analysis. In this prevention and management-oriented digital healthcare service, it is very important to develop a technology that can easily monitor a person's health status. One of the vital signs that can be used for personal health monitoring is blood pressure. High BP is a common and dangerous condition. About 1 out of 3 adults in the U.S. (about 75 million people) have high BP. This common condition increases the risk of heart disease and stroke, two of the leading causes of death for Americans. High BP is called the "silent killer" because it often has no warning signs or symptoms, and many people are not aware they have it. For these reasons, it is important to develop a technology that can easily and conveniently check BP regularly. In biomedical data analysis, various studies are being attempted to effectively analyze by applying machine learning to biomedical big data accumulated in large quantities. However, collecting blood pressure-related data at the level of big data is very difficult and very expensive because it takes a lot of manpower and time. So in this dissertation, we proposed a three-step strategy to overcome these issues. First, we describe a BP prediction model with extraction and

concentration CNN architecture, to process publicly disclosed sequential ECG and PPG dataset. Second, we evaluate the performance of the developed model by applying the developed model to privately measured data. To address the third issue, we propose the knowledge distillation method and input pre-processing method to improve the accuracy of the blood pressure prediction model. All the methods proposed in this dissertation are based on a deep convolutional neural network (CNN). Unlike other studies based on manual recognition of the features, by utilizing the advantage of deep learning which automatically extracts features, raw biomedical signals are used intact to reflect the inherent characteristics of the signals themselves.

keywords: machine learning, deep learning, cuff-less blood pressure measurement, convolutional neural network, biomedical signal analysis

student number: 2016-30209

Contents

List of Figures

List of Tables

Chapter 1

Introduction

Blood pressure (BP) is the pressure of circulating blood on the walls of blood vessels. Most of this pressure is due to work done by the heart by pumping blood through the circulatory system. BP is usually expressed in terms of the systolic blood pressure (SBP, maximum during one heartbeat) over diastolic blood pressure (DBP, minimum in between two heartbeats) and is measured in millimeters of mercury (mmHg), above the surrounding atmospheric pressure. Mean arterial pressure (MAP) is another value which represents the average BP in an individual during a single cardiac cycle [79]. BP is one of the vital signs, along with respiratory rate, heart rate, oxygen saturation, and body temperature. Normal resting BP, in an adult is approximately 120 millimetres of mercury (16 kPa) systolic, and 80 millimetres of mercury (11 kPa) diastolic, abbreviated "120/80 mmHg".

Disorders of BP control include hypertension, hypotension, and BP that shows excessive or maladaptive fluctuation. New guidelines for BP classification published by the American College of Cardiology and American Heart association in 2017 [71].

As can be seen in Table 1.1, normal BP is defined as a SBP of 90-119 mmHg or a DBP of 60-79. Hypotension is defined as a BP lower than the normal range, and

hypertension means a BP higher than the normal range. Arterial hypertension can be an indicator of other problems and may have long-term adverse effects. Sometimes it can be an acute problem, for example hypertensive emergency. Levels of arterial pressure put mechanical stress on the arterial walls. Higher pressures increase heart workload and progression of unhealthy tissue growth (atheroma) that develops within the walls of arteries. The higher the pressure, the more stress that is present and the more atheroma tend to progress and the heart muscle tends to thicken, enlarge and become weaker over time.

High BP is a common and dangerous condition. About 1 out of 3 adults in the U.S. (about 75 million people) have high BP. This common condition increases the risk of heart disease and stroke, two of the leading causes of death for Americans [44, 76]. High BP is called the "silent killer" because it often has no warning signs or symptoms, and many people are not aware they have it. Even moderate elevation of arterial pressure leads to shortened life expectancy. At severely high pressures, mean arterial pressures 50% or more above average, a person can expect to live no more than a few years unless appropriately treated [24]. Hypotension is low blood pressure. A SBP of less than 90 millimeters of mercury (mmHg) or DBP of less than 60 mm

Table 1.1: Blood Pressure classification in adults(Persons with systolic and diastolic in different categories are assigned to the higher category) [71]

Category	Systolic, mmHg	Diastolic, mmHg
Hypotension	<90	<60
Normal	90 - 119	60 - 79
Prehypertension (high normal, elevated)	120 - 129	60 - 79
Stage 1 hypertension	130 - 139	80 - 89
Stage 2 hypertension	>140	>90
Hypertensive crises	>180	>120
Isolated systolic hypertension	>160	<90 to 110

Hg is generally considered to be hypotension [41]. Hypotension is the opposite of hypertension, which is high BP. Severely low BP can deprive the brain and other vital organs of oxygen and nutrients, leading to a life-threatening condition called shock. For these reasons, it is important to check BP regularly.

Traditional BP measurement is based on the cuff. When using this method, BP cannot be re-measured until the occluded artery returns to its original position. It is not suitable for continuous BP measurement or observation of long-term BP change. The pressure of the cuff may also cause the subject to feel uncomfortable or to suffer skin trauma. To overcome these shortcomings, improvements in cuffless and continuous BP estimation methods have been an area of recent research [31, 66, 15, 21, 5].

Automated cuffless BP prediction is key to successful health care, but existing methods based on biomedical signal processing lack flexibility. Existing techniques are still being conducted to find additional features to help increase blood pressure prediction accuracy. For this, more manual feature extraction must be performed.

Another problem is the lack of publicly available datasets. To the best of our knowledge, there are two publicly published datasets. The first dataset, called PPG-BP database, contains PPG sugnals collected along with BP values from patients in china. It includes data collected from 219 subjects. Another dataset is the Multiparameter Intelligent Monitoring in Intensive Care (MIMIC) Database, which contain high resolution continuous recordings of physiological signals simultaneously collected such as arterial blood pressure (ABP), photoplethysmography (PPG), electrocardiography (ECG).

Data-driven approaches in analyzing biomedical signals, based on deep learning are being developed in areas such as nucleic acid sequence analysis [34, 46], electroencephalogram (EEG) analysis for measuring brain activity [10, 11], electronic medical record (EMR) [32, 47]. Convolutional neural network (CNN) surpasses the

previous approach to biomedical signal analysis and is becoming the primary method for biomedical signal analysis. However, collecting blood pressure related data at the level of big data is very difficult and very expensive because it takes a lot of manpower and time. In this dissertation, we proposed a three-step strategy to develop a BP prediction model while solving dataset-related problems.

- In Chapter 3, we describe a BP prediction model with extraction and concentration CNN architecture, to process publicly disclosed sequential ECG and PPG dataset.
- In Chapter 4, we evaluate the performance of the developed model by applying the developed model to privately measured data.
- In Chapter 5, we propose the knowledge distillation method and input preprocessing method to improve the accuracy of blood pressure prediction model.

All the method proposed in this dissertation are based on a deep convolutional neural network (CNN). Unlike other studies based on manual recognition of the features, by utilizing the advantage of deep learning which automatically extracts features, raw biomedical signals are used intact to reflect the inherent characteristics of the signals themselves.

Chapter 2

Background

Blood pressure is the pressure that blood exerts on blood vessels. The heart pumps blood to circulate every beat. As blood passes through the blood vessels, the elastic blood vessels expand to allow more blood to pass through each time the vessel wall is hit. In the subsequent relief phase, blood spreads to the peripheral parts of the body. Therefore, blood pressure is determined by the pumping power of the heart and its elasticity with the blood. During blood pressure measurement, blood pressure is measured as a periodic signal with maximum and minimum values depending on the heart rate. Systolic blood pressure is the highest arterial blood pressure value measured when the left ventricle contracts and the blood is pushed out of the heart and occurs near the end of the heart cycle. Diastolic blood pressure is the minimum arterial blood pressure value measured when the left ventricle is relaxed and the inside of the ventricle is filled with blood, and occurs near the beginning of the heart cycle.

According to the World Health Organization WHO, an adult-based cardiac systolic value (highest blood pressure) of 120 or less and a cardiac relaxation value (lowest blood pressure) of 80 or less are ideal. If your blood pressure value is over 140 or 90 over several days, you should consult a specialist. If hypertension is detected early,

it can be treated by improving your diet and lifestyle or through medication. Regular blood pressure measurement plays a critical role in early diagnosis. Blood pressure fluctuates under the influence of the subject's mental state or health status, so it is advisable to check it frequently. In some cases, the psychological effects of blood pressure measured at a medical institution and blood pressure measured at home or at work may be significantly different.

Arterial blood pressure is usually measured through a sphygmomanometer. Sphygmomanometer is a biometric medical device aimed at measuring blood pressure. The most relevant field of blood pressure measurement technology used today is illustrated in Figure 2.1. Sphygmomanometers traditionally used the height of the mercury column used to reflect the pressure of blood circulating through the body, starting from the heart. Although mercury is not used in devices or electronic devices that use aneroid barometers, which are mainly used recently, blood pressure values are still generally expressed in millimeters of mercury (mmHg). The sphygmomanometer can be roughly divided into Cuff-based methods and Cuffless methods depending on whether or not a cuff used for compressing blood vessels is used in measuring blood pressure.

Cuff-based methods are classified into auscultation method, oscillometric method, and tonometric method according to the measurement method. Auscultation method is a method of measuring blood pressure according to the Korotkoff sound using a stethoscope. A stethoscope is not necessary because the oscillometric method detects the heartbeat by calculating the systolic and diastolic blood pressure using the magnitude of the heartbeat from the blood vessel. Auscultation methods include mercury sphygmomanometers, aneroid sphygmomanometers, and hybrid sphygmomanometers. In cuff-based methods, to measure blood pressure, the cuff is worn on the forearm or wrist to compress blood vessels. This causes the artery to stop flowing for a

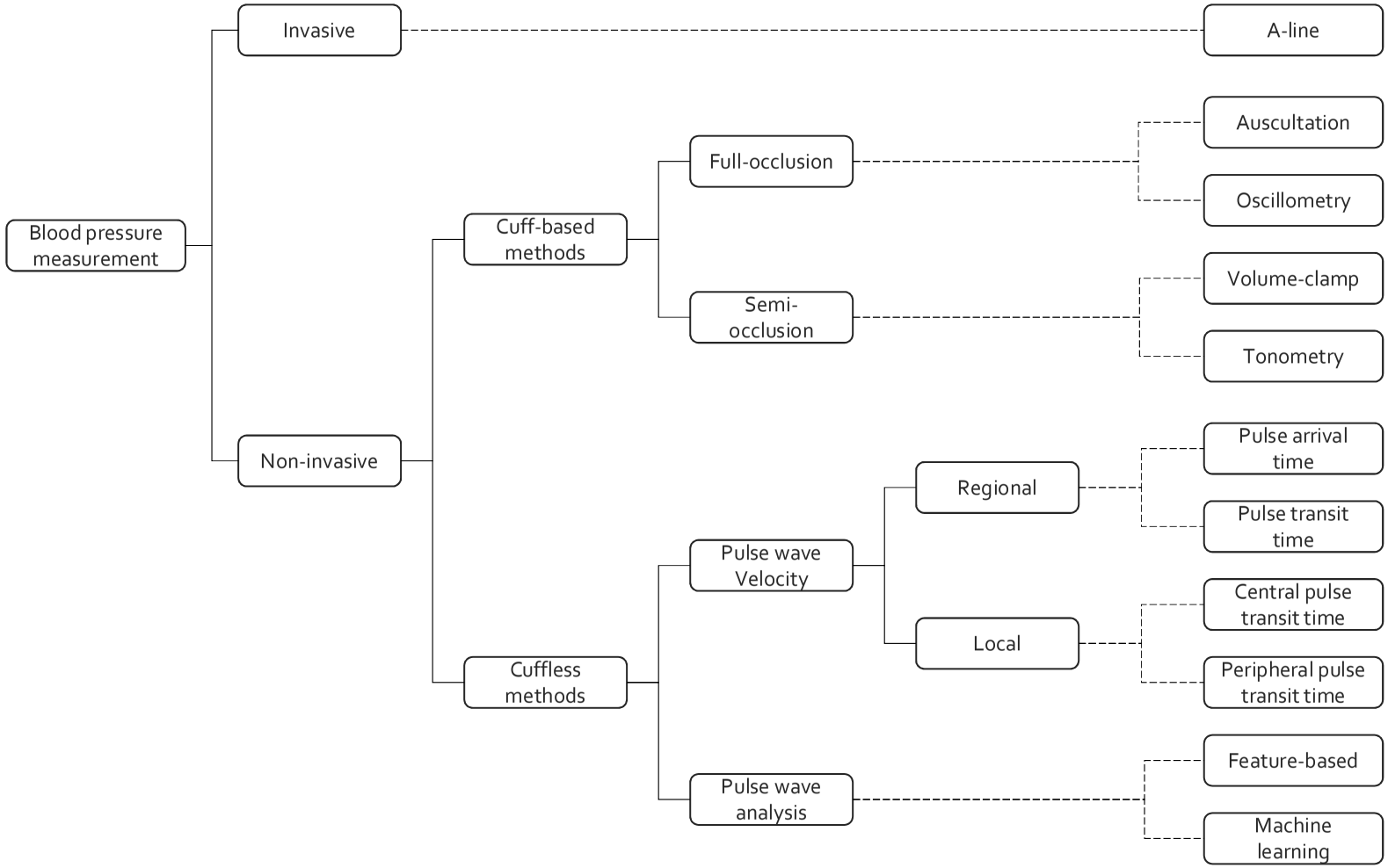

Figure 2.1: Blood pressure measurement classification.

short time.

The pressure of the cuff may also cause the subject to feel uncomfortable or to suffer skin trauma. There is a great demand for a cuffless BP measuring device that can solve these shortcomings, and sufficient advanced technology is required to develop it. The development of these devices allows us to measure blood pressure easily, continuously and accurately. Cuffless BP measurement is an all-inclusive term for a method that aims to measure BP without using a cuff. Current cuffless BP measurement devices use optical sensors, similar to fitness trackers are widely used by many people. The signal is usually measured by an optical sensor on the wrist or finger. Using these measured signals, systolic and diastolic blood pressure values are calculated through mathematical modeling. The advantage of this method is that you can measure blood pressure continuously without discomfort in your daily life. That's why it's especially useful for measuring blood pressure in the elderly or people with limited mobility. In addition, since most people own a smartphone equipped with a camera and motion sensor, blood pressure measurement through mobile healthcare is proposed as a solution for blood pressure management and early diagnosis.

2.1 Cuff-based BP measurement methods

2.1.1 Auscultatory method

A gold-standard method for non-invasive blood pressure measurement, developed by Riva-Rocci and Korotkoff in the early 20th century [55]. Auscultatory method measures blood pressure by the following method(Figure 2.2).

- After winding the cuff on the upper arm, apply pressure to the cuff to compress the brachial artery, preventing blood flow to the brachial artery.
- Place the stethoscope directly over the artery in the cuff.
- Slowly deflating the upper arm cuff until the first sound is heard from the stethoscope. The upper arm cuff pressure at this time is related to the systolic pressure.
- Slowly deflating the upper arm cuff until the sound disappears completely from the stethoscope. The upper arm cuff pressure at this time is related to the diastolic pressure.

The pressure actually applied to the upper arm cuff is measured by a mercury sphyg-

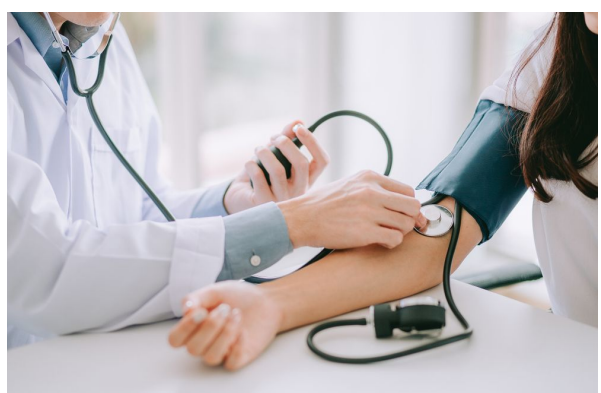

Figure 2.2: Auscultation example. From [12]

momanometer. It is also measured using a circular aneroid sphygmomanometer or an electronic pressure gauge. The auscultatory method requires the manipulation of a professionally trained medical practitioner(cuff contraction, interpretation of the Korotkoff sound), and there may be differences in measurement values between operators, which reduces the accuracy of blood pressure measurement. Therefore, regular operator training is required to achieve target measurement accuracy.

2.1.2 Oscillometric method

In order to overcome the shortcomings of the auscultation method, which had to be measured by a professionally trained medical practitioner, products that automatically measure blood pressure were introduced in the early 1970s [59]. The device, called an oscillometric device, replaces the Korotkoff sound auscultation with digital processing of pressure oscillations from the artery to the cuff. Oscillometric method measures blood pressure by the following method(Figure 2.3).

- Similar to the auscultation method, the cuff is wound around the forearm and then pressure is applied to prevent blood from flowing into the brachial artery.
- Slowly deflating the ambulatory cuff until there is diastolic pressure and record

Figure 2.3: Oscillometry example. From [12]

the pressure pulse from the brachial artery to the cuff.

- Systolic, diastolic, and mean blood pressure values are determined by time-series analysis of the recorded pressure pulses and the pressure applied to the cuff.

When reducing the pressure applied to the cuff, pressure pulses are maintained at systolic diastolic blood pressure, unlike the Korotkoff sound, which only sounds between diastolic and systolic blood pressure. Therefore, unlike the auscultation method, the oscillometric method cannot accurately measure systolic and diastolic arterial pressure. Nevertheless, the oscillometric method is an innovative device that can easily and repeatedly measure blood pressure without a well-trained and professional medical practitioner.

2.1.3 Tonometric method

In measuring blood pressure, arterial blood vessels are based on partial occlusion that only blocks a part of the artery, unlike the previous two methods, which must be completely closed [16]. Tonometric method allows the arterial pressure waveform to be continuously measured by well-positioning the sensing probe. First, the vessel is applied to the center of the artery until the vessel begins to distort. At this point, based on the linear spring model, the vertical displacement measured by the tonometer is proportional to the arterial pressure. Lastly, by consistently locating the tonometer, it is possible to continuously sense changes in the arterial pressure waveform. It is attractive because tonometric method can measure arterial waveforms continuously and accurately, but it has some limitations(Figure 2.4).

- The tonometry measures the vertical displacement value proportional to the arterial pressure. Therefore, the arterial pressure waveform can be recorded con-

Figure 2.4: Tonometry example. From [65]

tinuously, but the absolute blood pressure value cannot be measured. Therefore, tonometry is absolutely necessary to correct the blood pressure value measured by the auscultatory and oscillometric devices.

- In addition, the tonometer must be accurately centered in the artery and is very sensitive to subject movement.

Despite these drawbacks, it is considered a gold standard method to measure blood pressure non-invasively because it can continuously measure arterial waveforms.

2.2 Biomedical signals used in cuffless BP prediction methods

This section summarizes the theoretical background and usage of cardiovascular parameters used to predict blood pressure without cuffs. Biomedical signals covered in this section are electrocardiography (ECG), photo-plethysmography (PPG).

2.2.1 Electrocardiography (ECG)

Electrocardiogram (ECG) is a non-invasive bioelectric technology for observing the electrical activity of the heart from the outside. ECG can identify the pathological causes and nature of a heart by attaching several sets of electrodes to the skin's surface

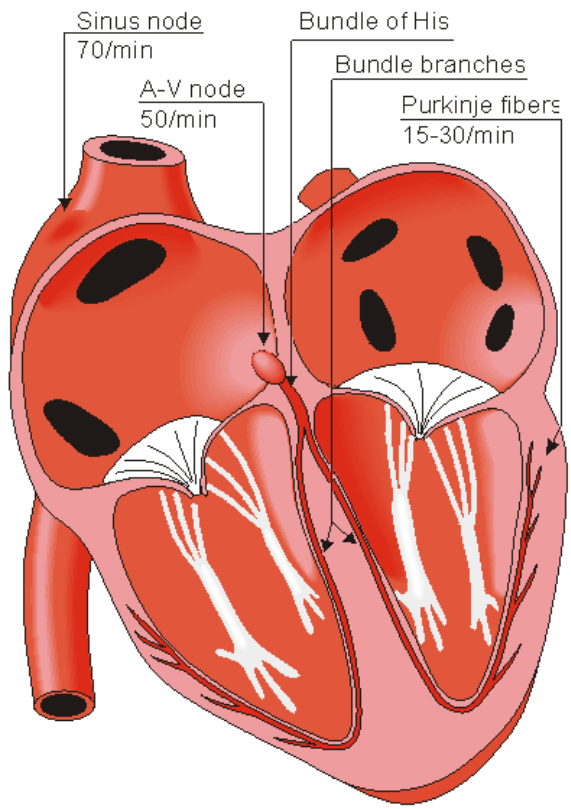

Figure 2.5: Electrical conduction system of the heart. From [43]

and observing the electrical properties produced by the heart cells during the heart cycle. The depolarization-repolarization cycle of the heart cells propagates through all heart tissue. The propagation of these electrical wave fronts is done through conductive fibers, allowing the heart to perform optimal pumping functions by adjusting the timing of contractions of different heart structures. A description of the heart's electrical delivery system is shown in Figure 2.5. The heart cycle is initiated by depolarization of the sinus node. At this point, electrical activation waves propagate to all myocytes in the vicinity, causing both atria to contract. When the electrical activation wave reaches the A-V node, the atrial-ventricular boundary, it is delivered to the bottom of both ventricles through the bundle of His and the Purkinje fibers. Afterwards, the contraction of ventricular myocytes moves upward. At various stages of the heart

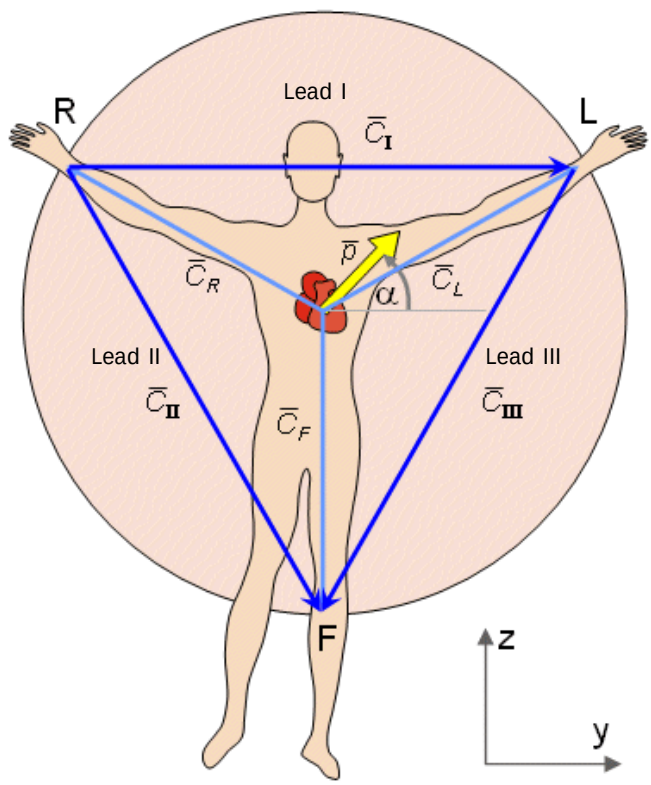

Figure 2.6: Definition of electrical limb leads. From [43]

cycle, the ionic currents produced by the heart propagates throughout the body. ECG is a technology for detecting these ionic currents on the skin surface. In 1908, W. Einthoven standardized a methodology for measuring these electrical signals. It was especially difficult to obtain estimates of electrical signals in 3D space. So he proposed a method to measure the projection of these vectors from three electrical limb leads(Figure 2.6).

- Lead I is the voltage between the (positive) left arm (LA) electrode and right arm (RA) electrode
- Lead II is the voltage between the (positive) left leg (LL) electrode and the right arm (RA) electrode
- Lead III is the voltage between the (positive) left leg (LL) electrode and the left arm (LA) electrode

Normally, cardiac function is tested through standard 12-lead ECG with 3 limb leads, 3 augmented limb leads (aVR, aVL, aVF) and 6 precordial leads (V1 to V6). Figure 2.7-2.10 shows the electrical characteristics of the heart projected onto three limb leads according to the heart cycle.

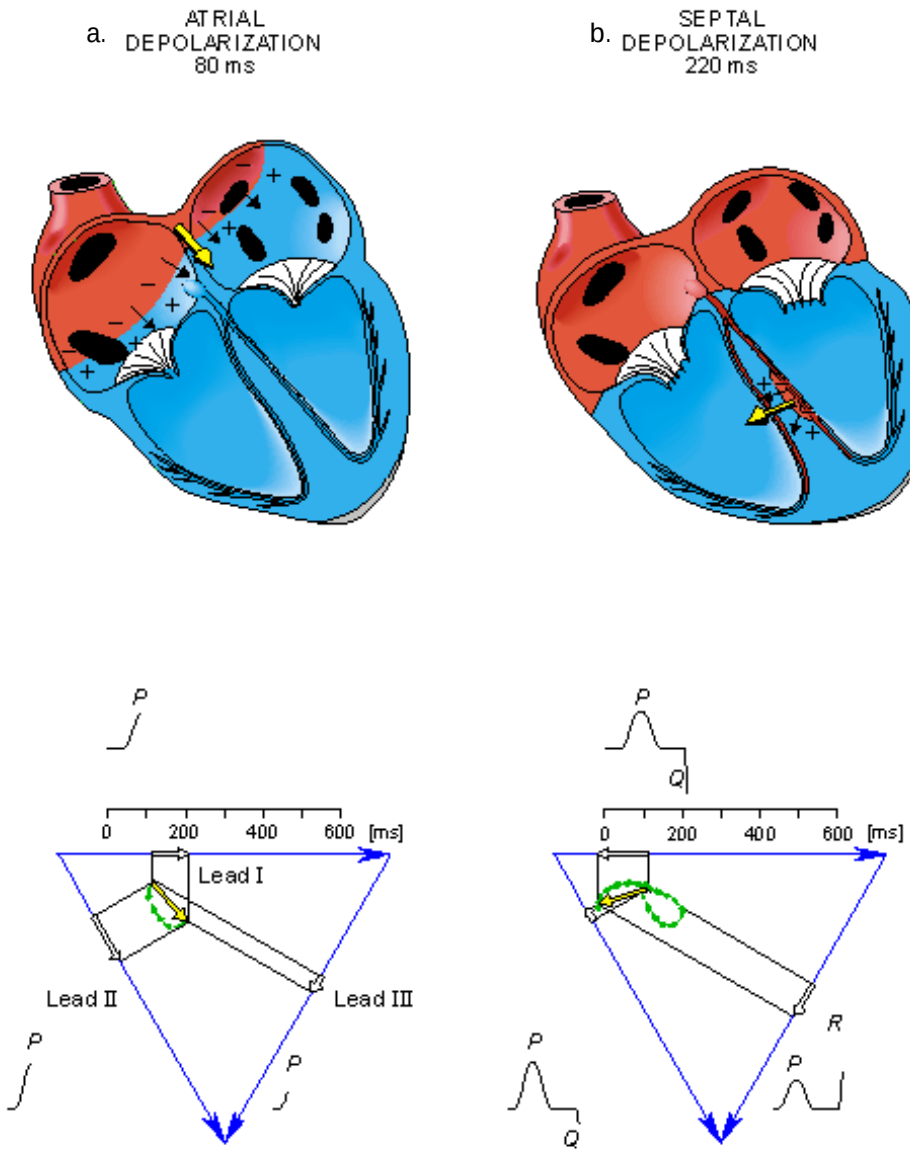

Figure 2.7: Genesis of ECG signals during full cardiac cycle.
a. Atrial depolarization. b. Septal depolarization. From [43]

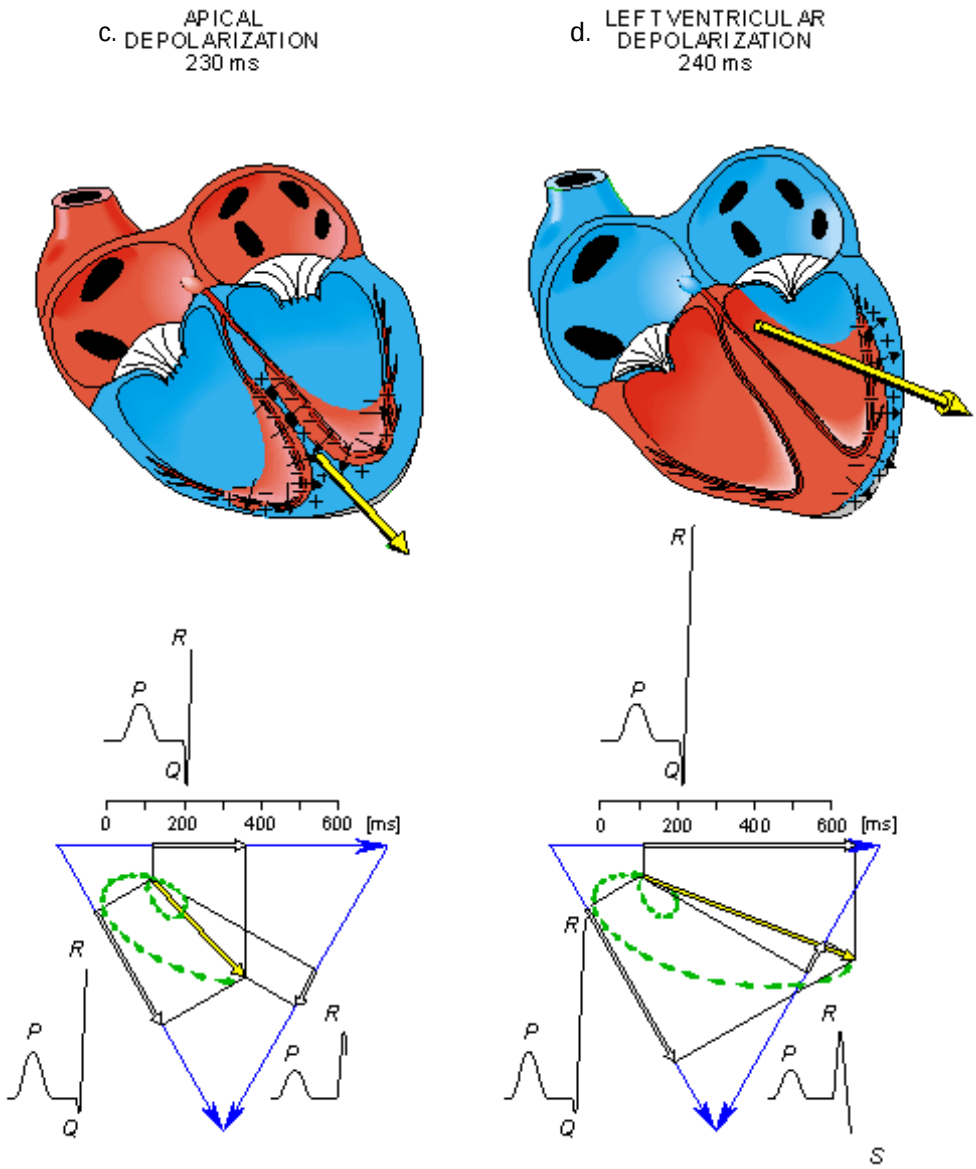

Figure 2.8: Genesis of ECG signals during full cardiac cycle.
c. Apical depolarization. b. Left ventricular depolarization. From [43]

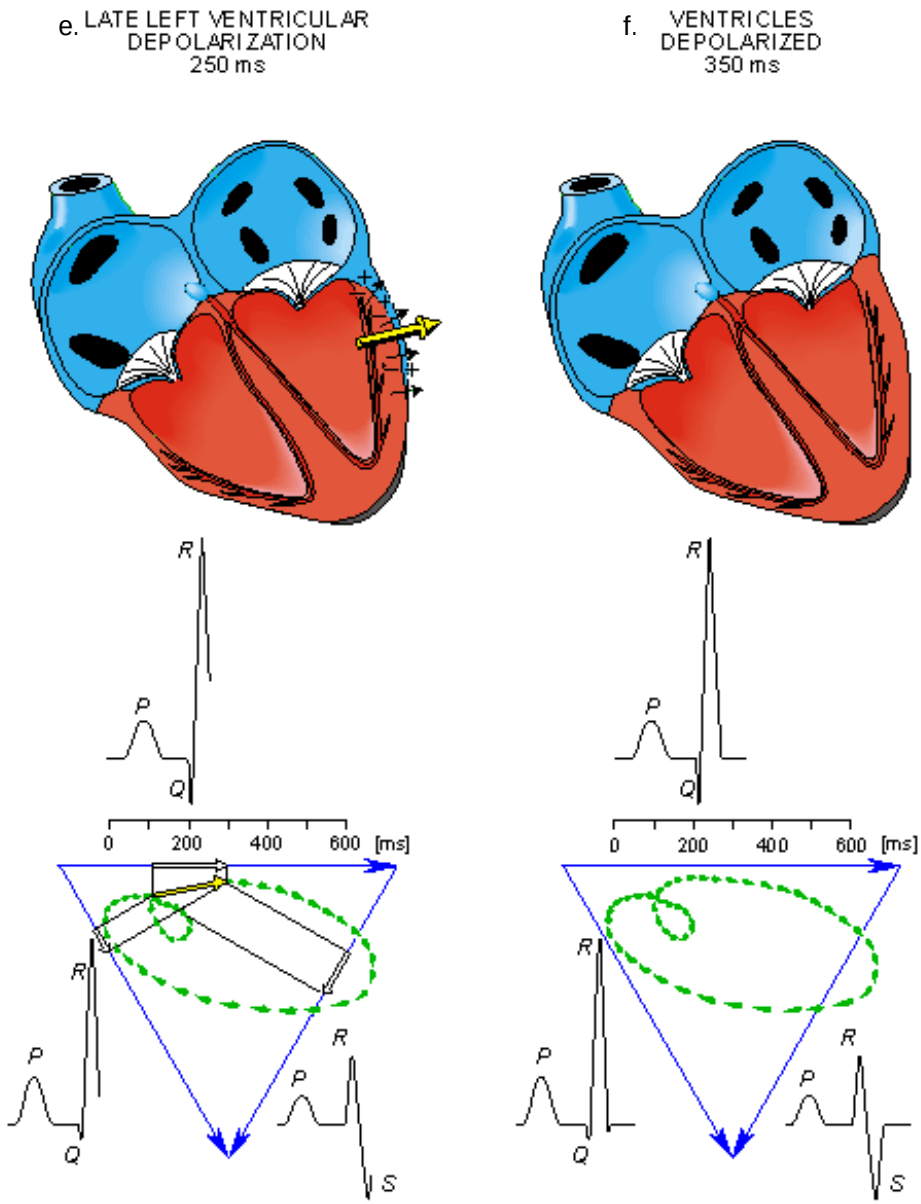

Figure 2.9: Genesis of ECG signals during full cardiac cycle.
e. Late left ventricular depolarization. f. Ventricles depolarized. From [43]

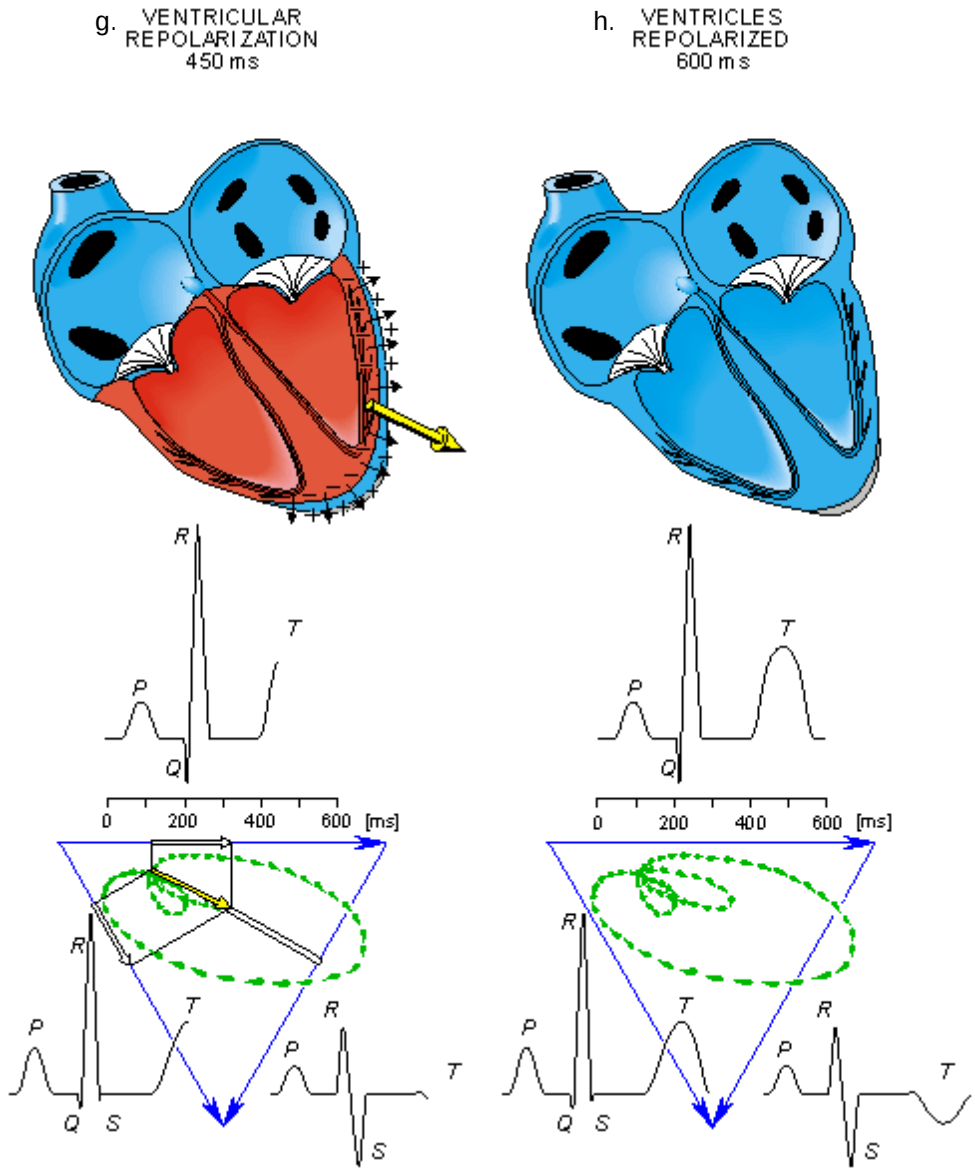

Figure 2.10: Genesis of ECG signals during full cardiac cycle.
g. Ventricular repolarization. h. Ventricles repolarized. From [43]

2.2.2 Photoplethysmography (PPG)

A photoplethysmogram (PPG) is a plethysmogram obtained using an optical method. It is mainly used to detect changes in microvascular blood volume in tissues. PPG is mainly measured using a pulse oximeter that illuminates the skin and measures changes in the amount of light absorbed. At every heart rate cycle, the heart pumps blood to external blood vessels outside the heart. This pressure pulse attenuates rather than the initial state when it reaches the distal skin, but is sufficient to dilate blood vessels in the tissue under the skin. The change in volume caused by this pressure pulse can be detected by illuminates light on the skin using an light-emitting diode (LED) and measuring the amount of light transmitted or reflected through the photo detector. Because blood flow to the skin can be regulated by several different physiological systems, PPG can be used to monitor heart rate and cardiac cycle, anesthesia depth, breathing, hypoglycemia and hypertension, blood pressure, and other circulatory conditions. The PPG waveform varies depending on the subject being measured, and also appears depending on the location and method of measurement.

2.3 Cuffless BP measurement methods

The classic method of measuring blood pressure without cuff is to find an indicator that reflects the change in BP value and indirectly measure the change in BP through measuring this indicator value. These indicators are non-invasive measurable features. For example, pulse transit time (PTT) is the most common indicator, and numerous studies have reported the relationship between PTT and blood pressure. There are many more indicators besides PTT. As shown in Table 2.1, algorithms and mathematical models have been proposed and developed to optimize the regression process of BP prediction and calibration of the PWV features/BP [64]. However, there are too many variables related to changes in blood pressure, and the relationship between each variable and blood pressure is too complex to express through simple physiologically-based mathematical modeling. Recently, as more data is available and computing power becomes stronger, many studies have been attempted to model the relationship between blood pressure-related indicators and blood pressure based on machine learning and deep learning technologies. These can be classified into two categories, PWV-based methods (with manual PWV features) and the non-PWV based methods.

Table 2.1: Summary of the PTT based cuffless BP measurement

First author	Model	Calibration (interval)	Reference method	Accuracy (mmHg) SBP	DBP
Young (1995)[77]	$SBP = a_1/PTT + b_1$ $DBP = a_2/PTT + b_2$	oscillometric BP (5min)	invasive radial BP	-0.37 (-29.0-28.2)	-0.01 (-14.0-14.8)
Chen (2000)[5]	$SBP = SBP0 - \frac{2}{\gamma PTT_0}(PTT - PTT_0)$	intermittent BP (5min)	invasive radial BP	RMSE: 3.70 $\pm$ 1.85	
Fung (2004)[20]	$BP = \frac{a}{PTT^2} + b$	cuff BP (10min)	cuff BP	-0.88 $\pm$ 11.32	
Poon (2005)[57]	$DBP = MBP_0 + \frac{2}{\gamma} ln \frac{PTT_0}{PTT} - \frac{1}{3} PP_0 \cdot \left(\frac{PTT_0}{PTT}\right)^2$ $SBP = DBP + PP_0 \cdot \left(\frac{PTT_0}{PTT}\right)^2$	cuff BP (initial)	average of auscultatory and oscillometric BP	0.6$\pm$9.8	0.9$\pm$5.6
Muehlsteff (2006)[49]	$SBP = a * lnPTT + b$ $SBP = a * L/PTT + b$	cuff BP (physical	cuff BP	RMSE:7.5 RMSE:6.9	

Table 2.1 continued from previous page

First author	Model	Calibration(interval)	Reference method	Accuracy (mmHg)	
				SBP	DBP
	$SBP = a * (L/PTT)^2 + b$	test)		RMSE:7.3	
Wong (2009)[72]	$SBP = a_1 * PTT + b_1$ $DBP = a_2 * PTT + b_2$	oscillometric BP (exercise, half/year)	oscillometric BP	0.0±5.3 half year: 1.4±10.2	0.0±2.9 half year: 2.1±7.3
Cattivelli (2009)[3]	$SBP = a_1 * PTT + b_1 * HR + c_1$ $DBP = a_2 * PTT + b_2 * HR + c_2$	invasive BP	invasive BP	-0.41±7.77	-0.07±4.96
Gesche (2011)[21]	$BP_{PTT} = P_1 \times PWV \times e^{(P_3 \times PWV)} + P_2 \times PWV^{P_4} - (BP_{PTTcal} - BP_{cal})$	cuff BP	cuff BP	SD:10.10	
Chen (2012)[6]	$SBP = b_{ij} e^{-(k_{ij/PWV_s})}$ $DBP = b_{ij} e^{-(k_{ij/PWV_d})}$	intra-arterial BP(9 subjects)	intra-arterial BP	1.49±6.51	2.16±6.23
Ding (2016)[14]	$SBP = DBP_0 \cdot \frac{PIR_0}{PIR} + PP_0 \cdot \left(\frac{PTT_0}{PTT}\right)^2$ $DBP = DBP_0 \cdot \frac{PIR_0}{PIR}$	finapres BP		-0.37±5.21	-0.08±4.06

Table 2.1 continued from previous page

First author	Model	Calibration(interval)	Reference method	Accuracy (mmHg)	
				SBP	DBP
Huynh (2018)[28]	$SBP = DBP_0 + B \cdot (D/PTT)^2$ $ln(1 + K(Z_{max0} - Z_{max}))$ $DBP = DBP_0 + B \cdot (D/PTT)^2$ $ln(1 + K(Z_{max0} - Z_{min}))$	oscillometric BP	oscillometric BP	RMSE: 8.47±0.91	RMSE: 5.02±0.73
Liu (2018)[40]	$MBP = HR * (k1 * DRPPG\,TD + b1)$ $PP = MBP * (k2 * t/HP + b2)$ $SBP = MBP = 2/3PP$ $DBP = MBP - 1/3PP$	Finapres BP		SD:2.85	SD:1.75

2.3.1 PWV based BP prediction methods

Studies have been carried out to improve BP prediction performance using the PWV-based features that were essential in traditional methods. BP refers to the pressure on the arterial wall when sending blood from the heart to the entire body. These arteries expand when the heart contracts (systole) and contract when the heart expands (diastole). The degree of expansion and contraction depends on the elastic modulus of the blood vessel. The following equation [62] expresses the relation between the elastic modulus of the blood vessel and the BP.

$$E = E_0 e^{\alpha_P} \tag{2.1}$$

In equation (2.1), E_0 and α are subject-specific parameters of central artery, P is BP.

Assuming that the artery is a connected elastic tube through which blood flows, the relationship between the velocity of the blood flowing along the artery and the elastic modulus of the blood artery is calculated using the Moens-Kortweg equation as follows:

$$PWV = \sqrt{\frac{hE}{\rho d}} \tag{2.2}$$

In equation (2.2), h and d are the thickness and diameter of the artery, respectively; ρ is the density of the blood.

Combining these two equations, we can obtain Bramwell-Hills and Moens-Kortweg's equation, explaining the relationship between BP and PWV, which is inversely proportional to the "Time Delay" for an artery with a length of L [69].

$$PWV = \frac{L}{TimeDelay} = \sqrt{\frac{hE_0 e^{\alpha_P}}{\rho d}} \tag{2.3}$$

These time delay values are known as PAT or PTT, and can be measured in a nonin-

vasive manner with various biomedical signals.

Kachuee [31] and Su [66] conducted a study to predict BP using PWV features as the main feature along with many other features extracted from biomedical signals. Kachuee extracted features from ECG and PPG signals and performed a study to predict BP in ECG and PPG signals using machine learning techniques, such as regularized linear regression (RLR), support vector machines (SVMs), decision tree regression, adaptive boosting (AdaBoost), and random forest regression (RFR). Mean absolute error (MAE) is used as an evaluation metric. The accuracy of BP prediction was found to be SBP 11.17 $\pm$ 10.09 and DBP 5.35 $\pm$ 6.14 for calibration-free, and SBP 8.21 $\pm$ 5.45 and DBP 4.31 $\pm$ 3.52 for calibration-based, respectively. Su extracted features from the ECG and PPG signals and performed a study to predict BP in ECG and PPG signals through recurrent networks (LSTM), which achieved SBP 3.73 and DBP 2.43 based on the root-mean-square error (RMSE).

2.3.2 Machine learning based pulse wave analysis methods

The non-PWV based method is a method of predicting the BP by analyzing the PWV signal itself, unlike the PWV-based method of extracting PTT-related features from the PWV in predicting the BP. So, it is usually called "pulse wave analysis". In the past, research has been conducted to find more suitable features for predicting BP in addition to PTT features. In recent years, as the amount of available data has increased and computing power has increased, as shown in table 2.2, many studies have been attempted to model the relationship between BP-related features and BP based on machine learning. Furthermore, studies are being conducted to predict BP at one time without extracting BP specific features using deep learning with end-to-end manner. There are studies on predicting the BP value or the Hypertension stage in the PPG and/or ECG signal using non-PWV based methods.

Table 2.2: Summary of the studies using machine learning-based cuffless BP prediction

Reference	Input features	Machine learning algorithm	Training and test	Performance
Xing et al. [74]	Spectrum amplitude and phase of PPG waveform	Artificial neural network with one hidden layer	69 subjects	SBP: 0.06±7.08 mmHg SBP: 0.01±4.66 mmHg
Sun et al. [67]	PPG and ECG signals, PAT and 18 PPG features from PPG and ECG signals	Multiple linear regression	19 subjects reference: Volume-clamp method Leave-on subject-out cross validation	SBP: 0.43±13.52 mmHg
Jain et al. [29]	32 parameters extracted from ECG and PPG	Sparse regression (to trim the redundant features)	Training: 99 subjects Test: 10 subjects Reference: OMRON HBP1300	SBP: MAD: 4.43 mmHg (SD: 4.90 mmHg) DBP: MAD: 2.46 mmHg (SD: 3.31 mmHg)
Duan et al. [17]	11 out 56 features from PPG signal	Support vector machine regression	57 subjects	SBP: 4.77±7.68 mmHg DBP: 3.67±5.69 mmHg MBP: 3.85±5.87 mmHg
He et al. [25]	18 features from ECG and PPG signals	Random Forest	One-hour continuous BP:1246 pairs DBP 1260 pairs SBP	SBP: 8.29±5.84

Table 2.2 continued from previous page

Reference	Input features	Machine learning algorithm	Training and test	Performance
Shobitha et al.[63]	18 features extracted from PPG signal	Relevance vector machine	26 subjects	SBP: Kappa score=0.99 DBP: Kappa score=0.99
Miao et al. [45]	14 features extracted from ECG and PPG	Multiple linear regression Support vector regression	73 subjects	SBP:-0.00±3.10 mmHg DBP: -0.00±2.20 mmHg
Lin et al. [39]	19 PPG indicators and PTT	Linear regression method	22 subjects	Combination of PPG and PTT achieves a better performance than PTT-based method
Su et al. [66]	7 features extracted from ECG and PPG signals	4 layer deep RNN (LSTM)	84 healthy subjects	SBP: 3.73 mmHg (RMSE) DBP: 2.43 mmHg (RMSE)
Ertugrul et al.[19]	ECG and PPG signals	Extreme learning machine	UCI dataset	SBP: 6.93 mmHg (MAE) MBP: 8.86 mmHg (MAE) DBP: 19.43 mmHg (MAE)
Radha et al.[58]	Activity features Heart rate variability PPG morphology features	A sequence-to-sequence model: perceptron + LSTM	120 subjects	SBP: 5.65 mmHg (RMSE)
Wang et al.[70]	Spectral and morphological features from PPG signal	Artificial neural network (one hidden layer)	72 subjects: 70% training 15% validation 15 % testing	SBP:4.02±2.79 mmHg DBP:2.27±1.82 mmHg
Ghosh et al.[22]	ECG and PPG	LSTM	50 health subjects	SBP 0.02 ±4.8 mmHg 1.5±3.7 mmHg

Table 2.2 continued from previous page

Reference	Input features	Machine learning algorithm	Training and test	Performance
Polinski et al.[56]	PTT, RR interval, and respiration signal	Single layer recurrent neural network	21 subjects	SBP: 1.06 mmHg(MAE) DBP: 0.63 mmHg(MAE)
Wu et al. [73]	Waveform information handcrafted features and personal features from ECG and PPG signals	Eight hidden layer deep neural networks	85 subjects	SBP: 3.63 mmHg(MAD) DBP: 2.45 mmHg(MAD)
Mousavi et al.[48]	Whole base features from PPG	Adaptive boosting regression	441 subjects	SBP:-0.05±8.90 mmHg MBP:0.07±4.91 mmHg DBP:0.19±4.17 mmHg

Khalid [33] extracted features from only PPG signals and performed a study to predict BP using machine learning techniques such as multiple linear regression (MLR), SVM, and decision tree regression. The accuracy of BP prediction was found to be SBP 4.82 $\pm$ 4.31 and DBP 3.25 $\pm$ 4.17. Wang [70] segments a single PPG signal from the raw PPG signal, extracts morphological and spectral features from the signal, and performs experiments to predict SBP and DBP through artificial neural networks (ANN), which achieved SBP 4.02 $\pm$ 2.79 and DBP 2.27 $\pm$ 1.82. Ertugrul [19] uses a spectrogram, which is the magnitude squared of the short-time Fourier transform (STFT) of a PPG and/or ECG signal, and then performed a study to predict BP through the extreme learning machine method (ELM). The accuracy of BP prediction was found to be SBP 4.37 and DBP 3.95. Zhang [78] also extracted features from a PPG signal and performed a study to predict BP using the SVM method, which achieved SBP 11.64 $\pm$ 8.20 and DBP 7.62 $\pm$ 6.78. Tanveer [68]

proposed a waveform-based hierarchical artificial neural network–long short-term memory (ANN–LSTM) model for BP estimation that automatically learns features from ECG and PPG signals through ANN and then uses them as inputs to LSTM to predict BP. Liang [38] transforms the PPG signal to a scalogram, which is a plotted RGB image as a graph of time and frequency, using a continuous wavelet transform. Hypertension classification was conducted using the pre-trained CNN (GoogLeNet). This study obtained superior hypertension classification performance compared to the studies considering PWV based features.

2.4 Deep learning for sequential biomedical data

Machine learning is a general-purpose artificial intelligence that can learn the relationship between data without considering the priority from data. It have the advantages that can derive a predictive model without a complete assumption about mechanisms that are usually hidden behind unknown or insufficiently defined mechanisms. In order to build a machine learning system, an engineering process or domain expertise were essential to convert raw data into a representation suitable for the learning system. Deep learning differs from traditional machine learning in the way that representaion is learned from raw data. The most differences between deep learning and traditional artificial neural networks are the number of hidden hidden layers, the connections between those hidden layers, and the ability to learn meaningful abstract concepts from inputs. It is different from traditional artificial neural networks, which are usually organized into three or so hierarchies and trained to obtain supervised representations by optimizing only for specific non-general tasks. All layers of the deep learning system optimize local non-supervised standards to express observed patterns based on data received as input from the lower layers. The main aspect of

deep learning is that these functional layers are not designed by human engineers, but are trained on data using universal learning procedures. In fact, deep learning was well suited to finding complex structures in high-level sequential data in medical domains such as genomics and biomedical signal processing, and natural language processing domains such as speech recognition, natural language understanding, and translation, and has achieved excellent performance. The deep architecture applied to each domain is mainly based on convolutional neural networks and recurrent neural networks.

2.4.1 Convolutional neural networks

Convolutional Neural Networks (CNN) has been mainly used in image related fields based on convolution precess and weight shared structure. The convolution layer performs convolution on the sub-sample layer using an arbitrary filter on the input signal, and then passes the result to the next layer. The next filtering is performed in the next layer, and through this process, it converge into a feature map that best reflects the characteristics of the input signal. In each convolution layer, a sub-region of the input is scanned through a learnable feature map called as filters. Through these learned filters, it is possible to find features that are locally related regardless of their location. Then, the features of the sub layer are concentrated and summarized through each pooling layer. CNNs are known to work effectively with all data with grid topology, as well as 2D data, such as video and image data. CNN shows excellent performance in the research using 2-dimentional data such as images and videos, as well as in the research using 1-dimentional form, such as studies predicting chromatin marks in DNA sequences [80] and studies predicting congestive heart failure in long-term electronic health records [7]. In particular, as in the case of TCN, prior studies have achieved good performance by applying a CNN to sequential 1D data.

2.4.2 Recurrent neural networks

Recurrent Neural Networks (RNN) is a type of artificial neural network that is connected by a directed (one-way) connection between hidden nodes unlike feed forward neural networks. Typically, an RNN consists of one network that does the same for all elements in the sequence, and each output value depends on previous calculations. Therefore, hidden nodes can affect all sub hidden nodes, and RNN can obtain long-term dependency between long data of sequential data. Based on these structural characteristics, it is known to show excellent performance as a model suitable for processing sequential data such as speech recognition, natural language understanding, and translation. In addition, to prevent vanishing and exploding gradient problems that can occur as time t increases, RNNs with gated recurrent unit (GRU) and RNNs with long short-term memory (LSTM) with gated state or memory have been developed. RNN shows excellent performance in studies dealing with sequential type biomedical data such as research predicting diagnoses and medications in patient history using RNNs with gated recurrent unit (GRU) [9] and research predicting future medical outcomes in current illness states using RNNs with long short-term memory (LSTM) hidden units [53].

Chapter 3

End-to-end blood pressure prediction via fully convolutional networks

Cardiovascular disease is the leading cause of death in the world. It is vital to prevent it by rapid diagnosis and appropriate management through periodic blood pressure (BP) measurement. Recently, many studies have been conducted on methods to measure BP without a cuff. One of the most common methods of predicting BP without a cuff is to use the correlation between pulse wave velocity (PWV) and BP. Studies that predict BP through PWV have two problems to overcome: 1) Additional efforts are required to extract PWV features manually from various biomedical signals, such as electrocardiogram (ECG) and photoplethysmogram (PPG); and 2) in predicting BP using biomedical signals from other people, individual periodic calibration is required because the correlation between PWV and BP differs from person to person. In this study, we proposed a cuffless BP prediction method based on a deep convolutional neural network (CNN) that can overcome the problems mentioned above.

The proposed CNN method 1) can use raw signals for training without PWV feature extraction; and 2) automatically learns the characteristics of biomedical signals from other people to predict BP accurately without calibration. We propose two schemes: extraction through multiple dilated convolution, and concentration through strided convolution with a large kernel, to process sequential ECG and PPG signals through CNN. BP prediction performance was the best when both ECG and PPG signals were used together. To this end, we conducted extensive experiments on the different settings of the proposed method and constructed an effective learning model. The proposed method achieved excellent performance in predicting both systolic blood pressure and diastolic blood pressure over other known approaches. We also verified that the performance of our method fulfills international standard protocols, AAMI, and BHS.

3.1 Introduction

High blood pressure (BP) is a common and dangerous condition. About 1 out of 3 adults in the U.S. (about 75 million people) have high BP. This common condition increases the risk of heart disease and stroke, two of the leading causes of death for Americans [44], [76]. High BP is called the "silent killer" because it often has no warning signs or symptoms, and many people are not aware they have it. For this reason it is important to check BP regularly.

Traditional BP measurement is based on the cuff. When using this method, BP cannot be re-measured until the occluded artery returns to its original position. It is not suitable for continuous BP measurement or observation of long-term BP change. The pressure of the cuff may also cause the subject to feel uncomfortable or to suffer skin trauma. To overcome these shortcomings, improvements in cuffless and continuous BP estimation methods have been an area of recent research.

Cuffless BP measurement is an all-inclusive term for a method that aims to measure BP without using a cuff. The most common method for cuffless BP measurement is based on manual examination of pulse wave velocity (PWV) features [31], [66]. PWV is the velocity of the pressure wave flowing through the blood vessels. This PWV based method can predict the blood pressure value by using the relationship between the time required for the blood to move between two points and the distance between these points. To measure the time value in a noninvasive manner, various biomedical signals, such as electrocardiogram (ECG), photoplethysmogram (PPG), ballistocardiogram (BCG) and seismocardiogram (SCG) are used [50]. A number of studies have shown that ECG and PPG signals are the most commonly used to effectively predict BP. The time values are referred to as pulse arrival time (PAT) or pulse transit time (PTT). PAT refers to the time difference between the R-peak of

the ECG signal and the PPG peak, and is usually obtained from the ECG signal and the PPG signal measured at one of the wrists, ankles, or other in vitro sites. PTT refers to the time it takes for a blood pressure-induced waveform to travel between two points in the artery, usually measured through PPG sensor signals. However, as described earlier in this paper, the PWV-based method requires recognizing features from the signal waveforms, and thus additional effort. This method also requires either a combination of simultaneously measured ECG and PPG or two simultaneously measured PPGs, which is inconvenient and cumbersome. Furthermore, the PWV-based method usually requires an elaborate individual calibration process using a sphygmomanometer with a cuff because the correlation between PWV features and BP varies from person to person [15], [21], [5] and thus cannot be used as a replacement for a cuff sphygmomanometer. There are some limitations with collecting ECG and PPG simultaneously using a mobile device.

As another way to predict BP without a cuff, some researchers have attempted to predict BP using a single raw biomedical signal or transform rather than the PWV-based feature [33], [70], [19], [78]. The concept of predicting BP using a single signal measurement such as ECG or PPG appears to be more appropriate for mobile devices such as smartphones and smart watches. A non-PWV based method can be relatively accurate without calibration because the method finds the characteristics which can predict BP in the biomedical signal itself without using the correlation between PWV and BP which is different from person to person. However, it is difficult to obtain high BP prediction accuracy using this method.

In this paper, we devised a method of BP prediction based on a deep convolutional neural network (CNN). The proposed method can overcome the drawbacks of feature recognition of the PWV-based method and the low BP prediction accuracy of non-PWV based method. It can take advantage of being a non-PWV based method with

relatively high BP prediction accuracy without calibration. Unlike other studies based on manual recognition of PWV features, by utilizing the advantage of deep learning which automatically extracts features, raw ECG and PPG signals are used intact to reflect the inherent characteristics of the signals themselves. It is also possible to predict relatively accurate BP without individual calibration.

The main contributions of our work are summarized as follows:

- We proposed a novel end-to-end method of predicting blood pressure using only raw signals with no hand-made features.
- Based on the architecture of CNN, our method has the flexibility to deal with input variations (PPG/ECG, Time/Frequency) and applicability to real-world situations.
- The proposed method achieved excellent performance in predicting both systolic and diastolic blood pressure using the MIMIC II dataset compared with other known approaches.

3.2 Method

We propose fully convolutional networks constructed using only 1D convolution for BP prediction. The proposed end-to-end 1D CNN model can predict SBP and DBP directly from raw signals without any additional manual feature extraction process, particularly PWV features.

A common deep learning approach for handling sequence data is to use recurrent-based neural networks. However, the signals related to BP (e.g., PPG, ECG, ABP) have a certain periodicity and pattern repetition, and so can be assumed to be grid topology data with wide range locality apart from long term time dependency. Therefore, we constructed a 1D convolution based neural networks to extract wide ranged local features from fixed length input signals and to regress the real numbered targets. The *Extraction-Concentration blocks* are key components of the proposed model, obtained by combining multiple dilated convolution and strided convolution using large kernel sizes [18]. It is possible to extract and concentrate features from the periodic signals.

The proposed BP estimation method consists of the following steps. 1) Data preparation: Prepare data pair (x,y) from the given database $\mathcal{D}$ for CNN training; 2) CNN based prediction model: Feature extraction through proposed *Extraction-Concentration blocks* and prediction with joint loss L_{total}.

3.2.1 Data preparation

Data sampling

The database $\mathcal{D}$ contains a set of raw PPG, ECG, and arterial blood pressure (ABP) signals $R_i = (r_i^{\text{PPG}}, r_i^{\text{ECG}}, r_i^{\text{ABP}})$, where i is the subject index and each R_i has a different length. For preparing the training dataset, we sampled random segments

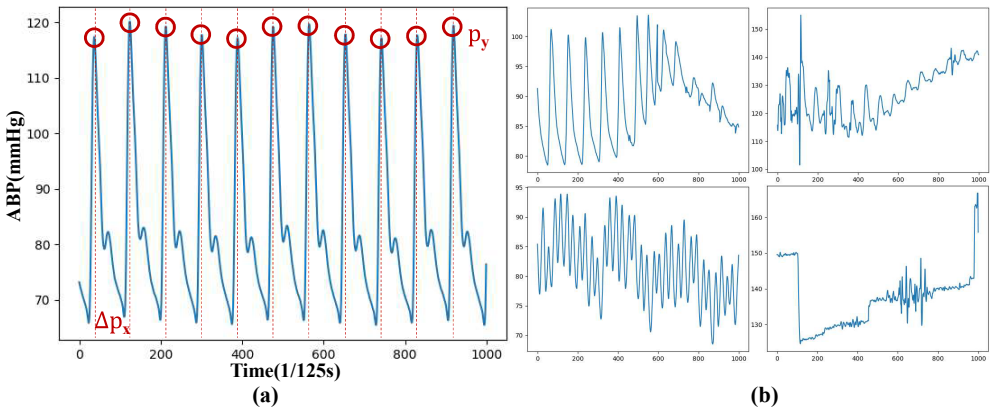

Figure 3.1: Examples of ABP signal for data sampling. (a) Illustration of the sampling constraints. (b) Examples of the false cases.

S_i from the raw signals to make all datasets the same length l_{seg}. Note that $l_{\text{seg}} = 1000$ for the experiments. During the sampling process, we applied two constraints to ABP signals (the true value of the estimation) for minimum refinement. According to NIH/WHO BP classification standard [8], we first apply the BP range criteria, $90 \leq \max(s^{\text{ABP}}) < 180$, $60 \leq \min(s^{\text{ABP}}) < 120$. Next, we exclude abnormal ABP signals through peak analysis, with the peak constraints defined as $\text{len}(p) \geq 5, \text{StdVar}(\Delta p_x) < 5, \text{StdVar}(p_y) < 5$, where peak $p = (p^1, .., p^n)$, p_x^i is the time stamp and p_y^i is the ABP value of the ith peak. Fig. 3.1 shows the sampling constraints and examples of excluded cases.

Preprocessing

Given segments S from the sampling process, we conducted the preprocessing steps to create adequate input and output data pairs for our method. Three preprocessing techniques are used: random cropping, fast Fourier transform (FFT), and increasing input depth using its derivatives. The preprocessing flow is illustrated in Fig. 3.2.

To increase the input variation, we use a randomly cropped signal X_t with length l_{in} in the l_{seg}-length segment S. Random cropping allows the model to learn signals

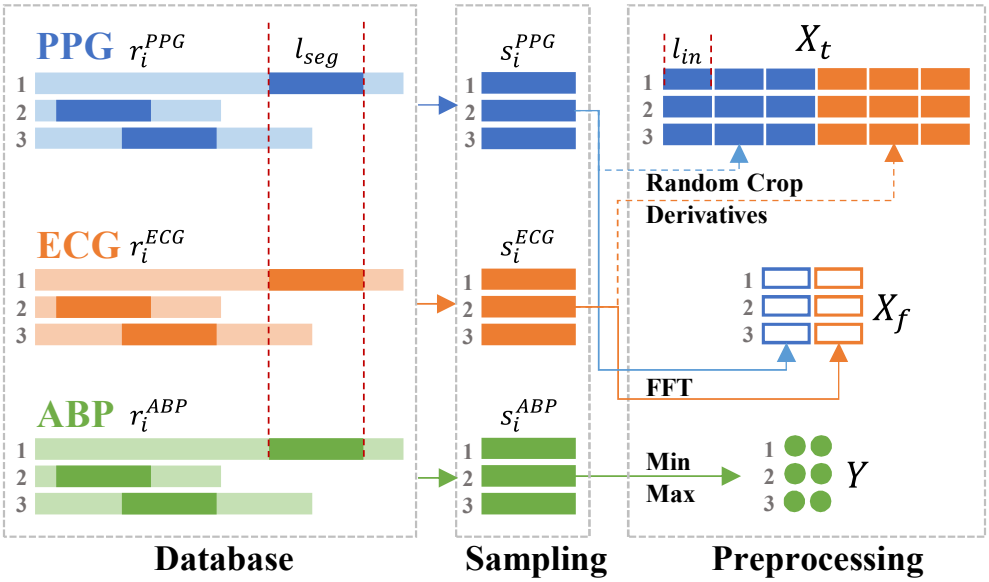

Figure 3.2: Data sampling and preprocessing flow.

at various points in the segment S and to reduce reliance on synchronization between signals. Note that we set $l_{\text{in}} = 512$ in the experiments. Since our model takes both time and frequency domain inputs, the original signal needs to be converted to the frequency domain. FFT is used at this stage; we use Fourier spectrum X_f from the original signal X_t as the input for the frequency encoder. Next, for time domain signals, we increase the input depth by concatenating the input signal's 1st and 2nd derivatives as follows [37].

$$X_t = X_t \oplus \Delta X_t \oplus \Delta^2 X_t \tag{3.1}$$

The accuracy difference according to the input signal's derivative are shown in chapter 3.3.2.

After the preprocessing step, we end up with a prepared dataset (X_t, X_f, Y) from which we take a mini-batch (x_t, x_f, y) for model training. The dimensions of the prepared dataset in the experiments are $m \times 6 \times 512$, $m \times 2 \times 256$, $m \times 2$ with

mini-batch size m for x_t, x_f, y, respectively.

3.2.2 CNN based prediction model

The overall architecture of the proposed method is shown in Fig. 3.3. It consists of three parts: a time encoder, a frequency encoder, and three predictors for time, frequency, and combined feature matrices. The time encoder $h_t(\cdot)$ learns representative features in time-series inputs x_t, and outputs the corresponding feature matrix z_t. In parallel with the time encoder, the frequency encoder $h_f(\cdot)$ outputs feature matrix z_f for the frequency domain inputs x_f. Each encoder is composed by stacking two core modules named *Extraction* and *Concentration blocks*, which are designed to learn effective latent features from the data with periodicity.

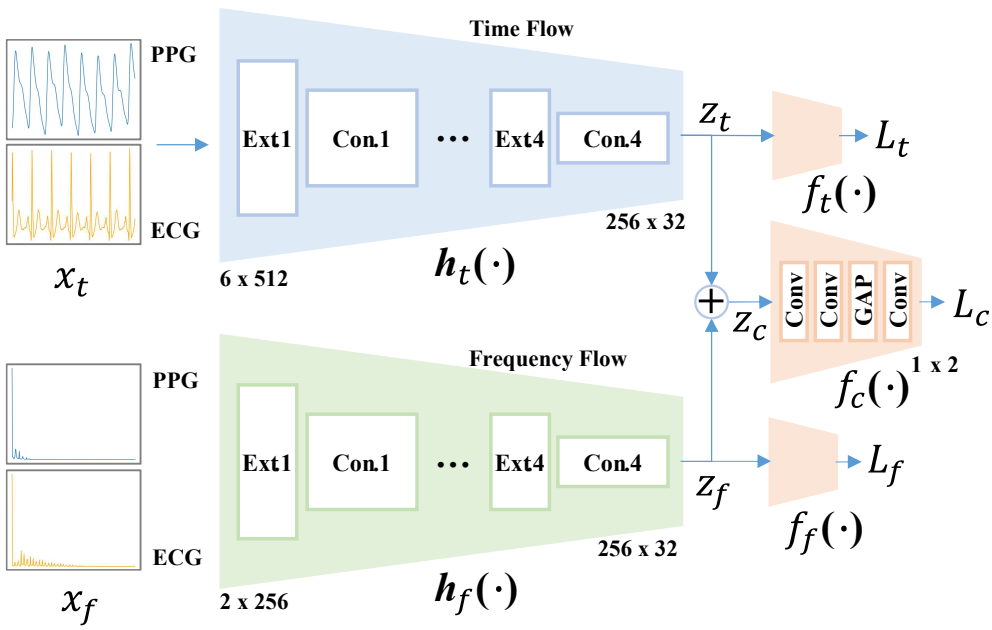

Figure 3.3: Overview of the proposed BP prediction model based on fully convolutional neural networks.

Extraction-Concentration Blocks

For CNN to handle periodic sequential data, such as PPG and ECG, the main issue is how the model can learn the relationship between neighboring data points with different intervals unlike images. Two components, multiple dilated convolution and strided convolution with a large kernel, are the main features of our method. We illustrate the detailed structure of *Extraction* and *Concentration blocks* in Fig. 3. 4.

In the *Extraction block* $E(\cdot) : \mathbb{R}^{D\times W} \rightarrow \mathbb{R}^{D\times W}$, where D is the input dimension, and W is the size of input, we use four parallel dilated convolutions with pre-defined kernel size k_{EXT} and dilation factors of [1, 2, 3, 4]. A model can learn the various relationships between different neighboring pixels within the $4 \times (k_{\mathrm{EXT}} - 1) + 1$ range

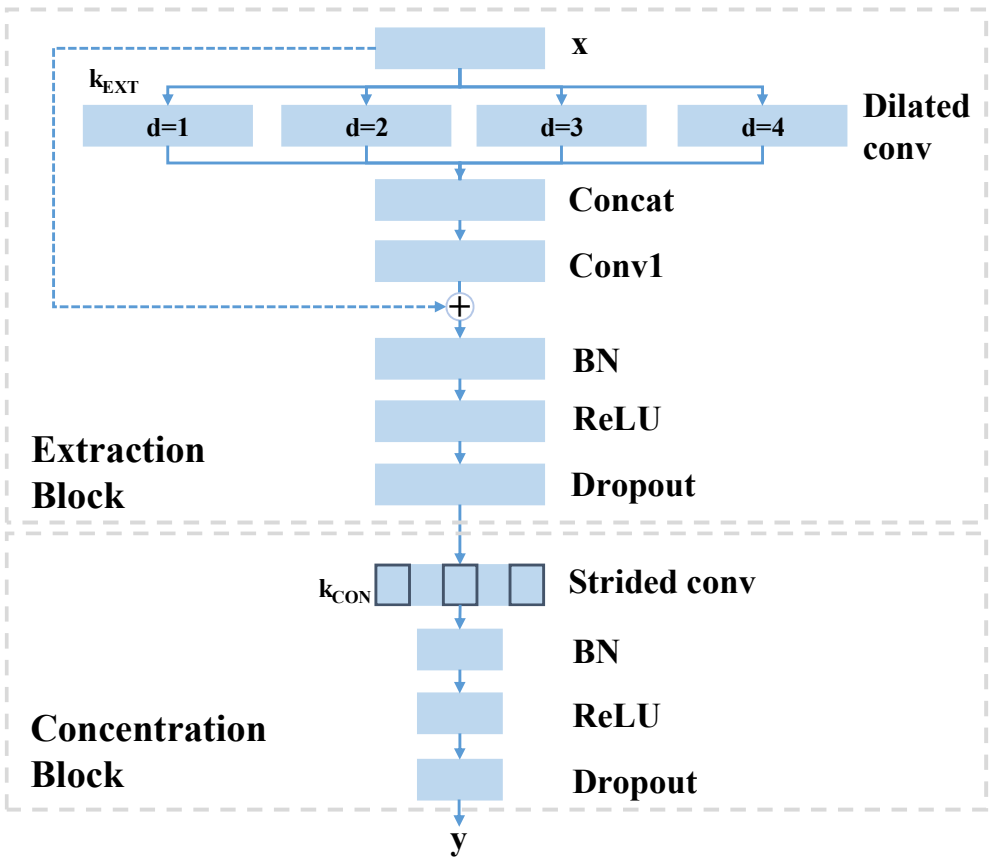

Figure 3.4: Detailed architectures of *Extraction* and *Concentration* blocks.

through multiple dilated convolution. Each output from the multiple dilated convolutions is concatenated together and reduced to the initial dimension by convolution with filter size 1. We use the residual connection, which is a well-known technique to allow better gradient flow. As with temporal convolutional networks (TCN), the combination of batch normalization (BN), ReLU non-linearity, and dropout layer is placed after the residual connection [2].

In the *Concentration block* $C(\cdot) : \mathbb{R}^{D \times W} \rightarrow \mathbb{R}^{D' \times \frac{W}{2}}$, where D is the input dimension, D' is the output dimension, and W is the input size. The model can concentrate the outputs from the *Extraction block* and increase the depth of the features to gain better representations, which lie in a lower dimension space. A typical choice for this concentration is max pooling, but we use a strided convolution with kernel size k_{CON} as an alternative. The reason for this is because there is much information loss by pooling when we apply a large kernel size. We compare the performance between pooling and strided convolution through the experiment in chapter 3.3.2. After the strided convolution, the BN+ReLU+Dropout combination layer is placed in the same way as the *Extraction block*.

Both the time encoder and the frequency encoder consist of four *Extraction* + *Concentration* combinations. Another important factor here is the receptive field size. Even though the network is deeply stacked to increase the receptive field, the actual network has a characteristic of focusing on local regions [42]. Therefore, we chose to increase the kernel size instead of deeply configuring the network. Considering the possible heart rate range, an input signal of more than 4 seconds can contain at least 2 periods of the signal, which implies that the input needs to have 500 pixels when using a 125 Hz sampling frequency. The proposed model should therefore have a receptive field size of more than 500 pixels. More precisely, since the inputs to our model have sizes of 512 and 256 for the time and frequency domain respectively, the

kernel sizes of each *Extraction* (k_{EXT}) and *Concentration blocks* (k_{CON}) are needed to satisfy these constraints. Possible combinations of the filter sizes for our 4-EC stacked networks are (3, 27, 25), (5, 19, 17) and (7, 11, 9) for $(k_{\mathrm{EXT}}, k^t_{\mathrm{CON}}, k^f_{\mathrm{CON}})$, where k^t_{CON} and k^f_{CON} are the filter sizes of the *Concentration block* for time and frequency flow. We selected (7, 11, 9) for the experiments, and related results regarding filter sizes will be described in chapter 3.3.2.

Prediction and Training

After feature extraction through both time and frequency encoders, we can define the combined feature matrix $z_c = z_t \oplus z_f$. The combined predictor $f_c(\cdot) : \mathbb{R}^{D_c \times W} \rightarrow \mathbb{R}^2$, where D_c is the dimension of z_c and W is the size of z_c, consists of a double stacked convolution layer, global average pooling, and a dimension reduction convolution layer. The output $\hat{y}_c$ of $f_c(\cdot)$ is two real numbers which indicate SBP and DBP. The objective of the prediction is to minimize the distance between the target y and the prediction y_c. L1 and L2 distance are the typical error measurements; we compared the performance of both cases applying the L1 or L2 distance in chapter 3.3.2. The objective to minimize is defined as:

$$L_c = d(y_c, \hat{y_c}), \tag{3.2}$$

where d can be any distance metric between real numbers, L1 and L2 in this case.

In addition to this, we added two auxiliary flows from the predictors $f_t(\cdot)$ and $f_f(\cdot)$ which take the pre-concatenated features z_t and z_f as inputs, respectively. Both auxiliary predictors have a simpler structure which consists of one convolution layer, global average pooling, and a dimension reduction convolution layer. Auxiliary loss is a well-known technique to help the model's gradient flow in the back-propagation

phase, and will improve performance. We introduce the importance factor α to both losses L_t and L_f. Our final loss is defined as follows:

$$L_{\text{total}} = L_c + \alpha(L_t + L_f) \tag{3.3}$$

The effect of auxiliary loss will be described in chapter 3.3.2. We can update the model parameters by mini-batch gradient descent with respect to the current model weight. Training details for the experiments will be outlined in chapter 3.3.1.

3.2.3 Detailed architecture

Table 3. 1 shows detailed information about the proposed architecture. It contains the layer structure, input/output dimension, size of kernel/stride/dilation and the receptive fields at each layer.

Table 3.1: Model architecture details

Arch	Layer	Operation	Size	Out	Kernel	Stride	Dilation	Recep. field
Time	*Ext.1*	Multi-conv	6x512	6	7	1	[1,2,3,4]	25
		BN+ReLU+Dropout						
	Con.1	Conv	6x512	32	11	2	1	35
		BN+ReLU+Dropout						
	Ext.2	Multi-conv	32x256	32	7	1	[1,2,3,4]	83
		BN+ReLU+Dropout						
	Con.2	Conv	32x256	64	11	2	1	103
		BN+ReLU+Dropout						
	Ext.3	Multi-conv	64x128	64	7	1	[1,2,3,4]	199
		BN+ReLU+Dropout						
	Con.3	Conv	64x128	128	11	2	1	239
		BN+ReLU+Dropout						
	Ext.4	Multi-conv	128x64	128	7	1	[1,2,3,4]	431
		BN+ReLU+Dropout						
	Con.4	Conv	128x64	256	11	2	1	511
		BN+ReLU+Dropout						
Freq	*Ext.1*	Multi-conv	2x256	2	7	1	[1,2,3,4]	25
		BN+ReLU+Dropout						
	Con.1	Conv	2x256	32	9	1	1	33
		BN+ReLU+Dropout						
	Ext.2	Multi-conv	32x256	32	7	1	[1,2,3,4]	57
		BN+ReLU+Dropout						
	Con.2	Conv	32x256	64	9	2	1	65
		BN+ReLU+Dropout						
	Ext.3	Multi-conv	64x128	64	7	1	[1,2,3,4]	113
		BN+ReLU+Dropout						
	Con.3	Conv	64x128	128	9	2	1	129
		BN+ReLU+Dropout						
	Ext.4	Multi-conv	128x64	128	7	1	[1,2,3,4]	225
		BN+ReLU+Dropout						
	Con.4	Conv	128x64	256	9	2	1	257
		BN+ReLU+Dropout						
Comb	Layer1	Conv	512x32	512	3	1	1	
		BN+ReLU+Dropout						
	Layer2	Conv	512x32	512	3	1	1	
		BN+ReLU+Dropout						
	Layer3	GAP	512x32	512x1				
		Conv	512x1	2	1	1	1	

3.3 Experimental results

3.3.1 Setup

In the experiments, the Cuffless Blood Pressure Estimation dataset is used as a source of the ECG, PPG, and ABP signals. This dataset was generated by Kachuee [30], initially collecting ECG, PPG and ABP signals from the Physionet's Multi-parameter Intelligent Monitoring in Intensive Care (MIMIC) II (version 3, accessed on Sept. 2015) online waveform database [61] and then preprocessing to remove the deterioration effects of noise and artifacts from the raw signals. The dataset consists of 12,000 records with all of the ECG, PPG, and ABP signals in hierarchical data format. Each record consists of three rows, with each row corresponding to one signal channel: 125Hz ECG from channel II (ECG lead II), 125Hz PPG from a fingertip, 125Hz invasive ABP. After the data preparation process described in chapter 3.3.1., the entire dataset contains 1,912 records from 942 different subjects. We split the dataset into training (70%, 1,340), validation (10%, 193), and test (20%, 379) sets.

For training, we use the Adam optimizer with $\beta_1 = 0.9,\ \beta_2 = 0.999$, a mini-batch size of 100, and no weight decay. The initial learning rate is 0.001 decayed by 0.2 after 800 epochs. The dropout rate is set to 0.2 for the entire networks.

3.3.2 Model evaluation & selection

To investigate the effect of model parameters, we performed prediction error analysis with changes in different components (e.g., loss metric change, the weight of auxiliary loss, type of pooling, kernel size). Fig. 3.5, 3.6, 3.7. shows the difference in prediction error value according to loss metric change (L1, L2), weight of auxiliary loss (0, 0.2, 0.4, 0.6), type of pooling (Strided Conv, MaxPool, AvgPool), and kernel size (filter combination).

As can be seen in Fig. 3.5, in the case of using L1 loss, the prediction error is lower than that using L2 loss. In the case of auxiliary loss weight α, a small auxiliary loss weight helps the model's gradient flow in the back propagation phase, which reduces the prediction error. If a large weight is used, however, the prediction error is increased because L_t and L_f have a greater impact on L_{total} than L_c.

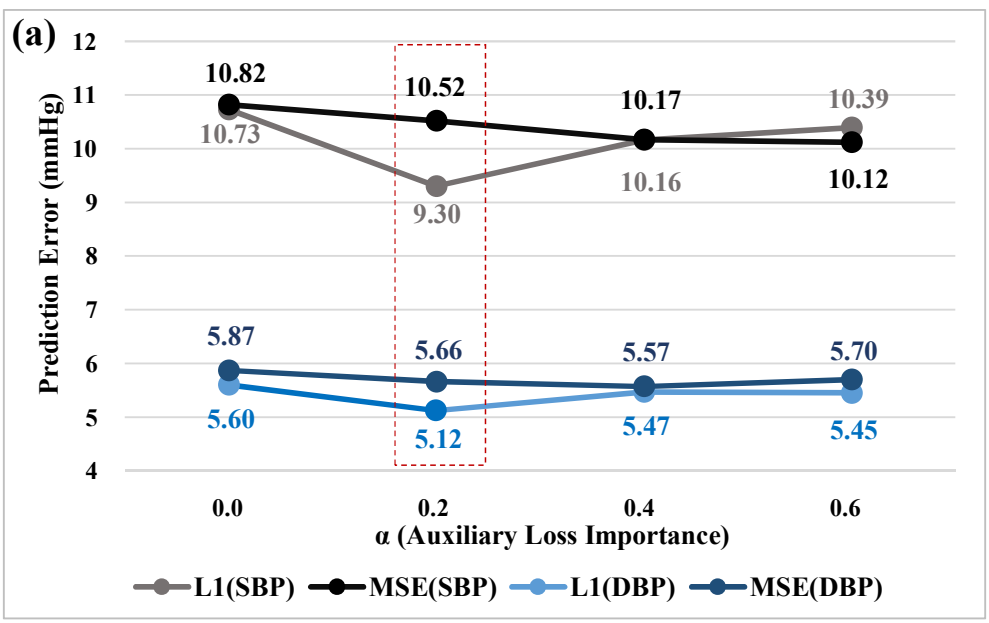

Figure 3.5: BP prediction error analysis according to the model component changes. The best performing model is marked with a red dotted line. (a) BP prediction error due to loss metric and auxiliary weight variation.

The results of the prediction error measurement depending on the pooling type and the kernel size can be seen in Fig. 3.6. In the case of the pooling type, it can be confirmed that the prediction error when using Strided Conv is lower than that when using MaxPool or AvgPool. This is due to the information loss by pooling when we apply a large kernel size. In the case of the combination of filter sizes, we conducted an experiment to compare prediction error for three combinations. It was confirmed that the prediction error of the $k_{\mathrm{EXT}}, k^t_{\mathrm{CON}}, k^f_{\mathrm{CON}} = 7, 11, 9$ combination with the largest k_{EXT} is the lowest because the model can learn the relationship between pixels in a larger neighborhood through a large k_{EXT}.

The results of the BP prediction error test with and without input signal's deriva-

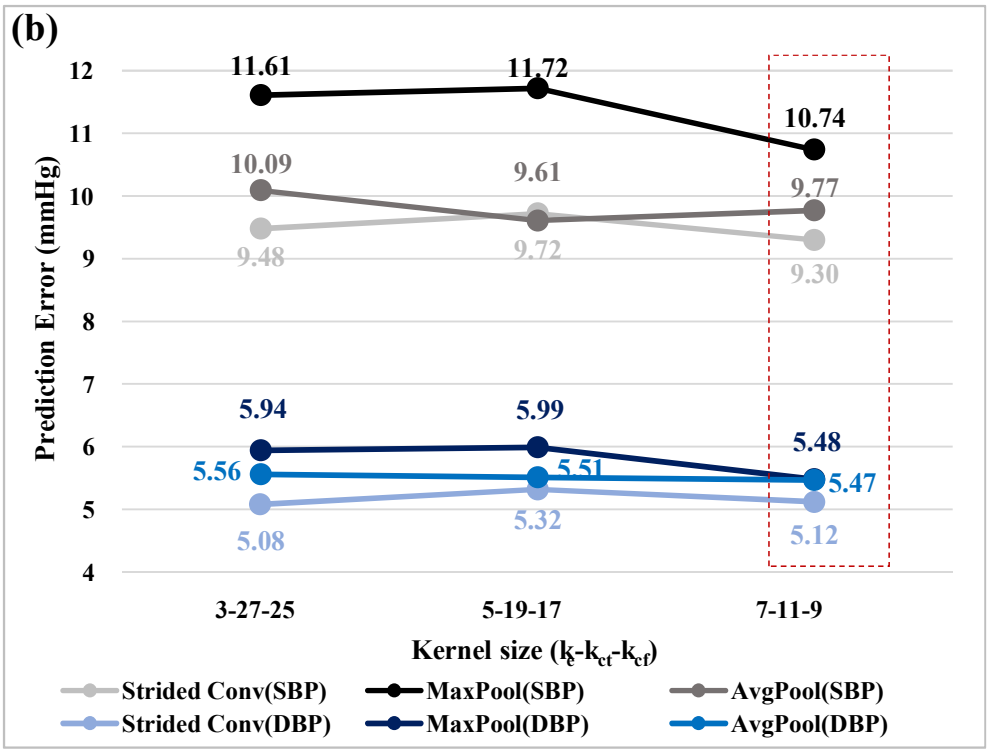

Figure 3.6: BP prediction error analysis according to the model component changes. The best performing model is marked with a red dotted line. (b) BP prediction error according to pooling type and kernel size.

tive are shown in Fig. 3.7. BP prediction error is lowest when input signal's first and second derivatives are used together with the original signal regardless of the calibration. Through prediction error analysis with component changes, SBP and DBP prediction performance are the best when using L1 loss, a weight of auxiliary loss α = 0.2, Strided Conv, and a combination of $k_{\mathrm{EXT}}, k^t_{\mathrm{CON}}, k^f_{\mathrm{CON}}$ = 7, 11, 9. BP prediction performance results are shown in Table 3.2 with the calibration-based results to be covered in the next chapter.

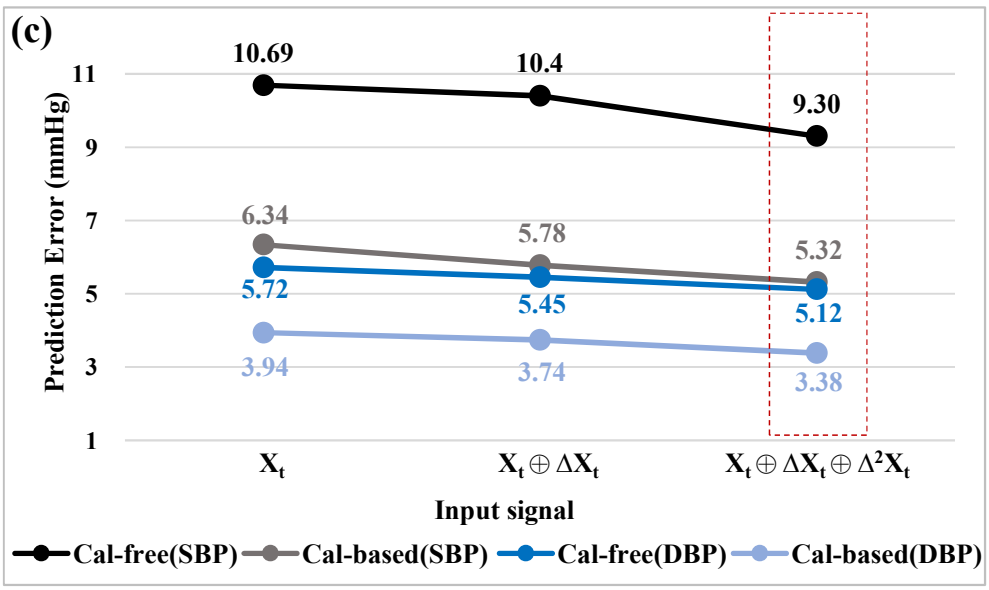

Figure 3.7: BP prediction error analysis according to the model component changes. The best performing model is marked with a red dotted line. (c) BP prediction error due to the use of derivatives of the input signals.

3.3.3 Calibration-based method

The proposed method in this study does not need any calibration to predict BP. However, when using a smart device, such as a telephone or a watch, to repeatedly measure data to estimate the BP, it is possible to improve the accuracy of BP prediction by calibrating the pre-trained models using partial personal data. To confirm the improvement of the BP prediction accuracy of the calibration based method, test data was divided into several non-overlapping sections. Half of the divided data is used for calibrating the pre-trained model and the remaining data is used to evaluate the BP predictive ability of the calibration-based model.

Fig. 3.8. presents the scatter plots for calibration-free and calibration-based methods, when using the best performance model as selected in the previous chapter.

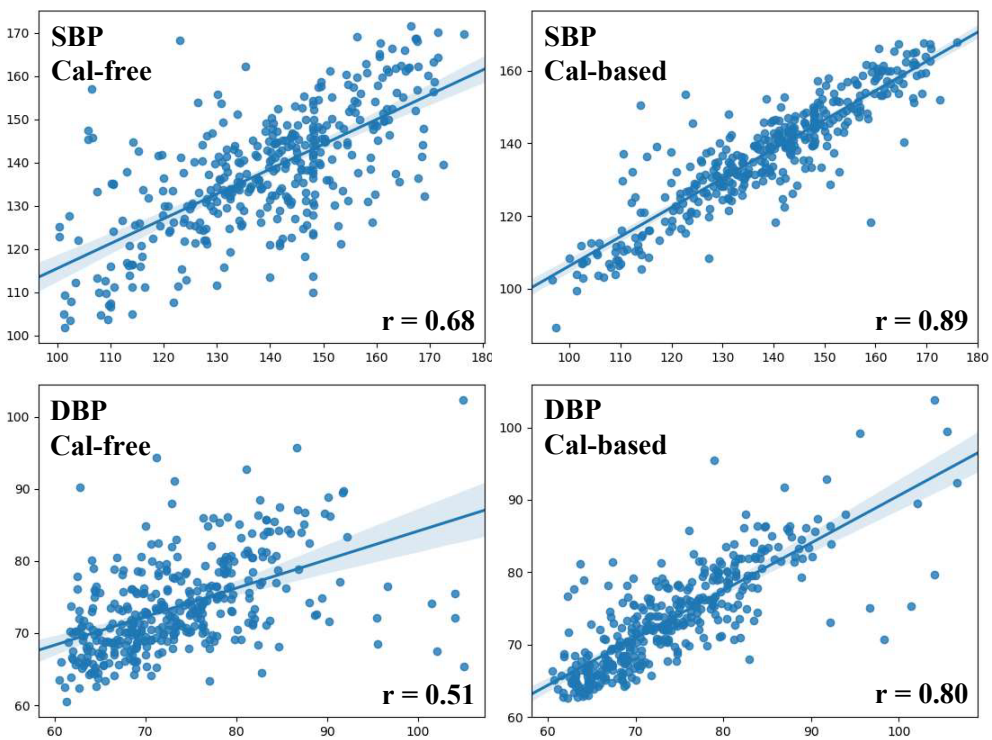

Figure 3.8: Scatter plots for calibration-free and calibration-based models. The x-axis represents the reference value and the y-axis represents the predicted value.

When comparing the graphs before and after calibration, the scattered points on the graph converge to a straight line through calibration, which can also be confirmed by comparing Pearson's correlation coefficient (r) values before and after calibration in both SBP and DBP. In particular, calibration-based model showed a high Pearson's correlation coefficient of SBP 0.89, DBP 0.80, which are higher than those shown in other experiments using PWV features (PAT, PTT and so on) and MIMIC dataset [36]. The Pearson's correlation coefficient between blood pressure and PWV features was reported as a value between -0.28 and -0.71. We have confirmed that the features extracted automatically through CNN proposed in this paper are more suitable for predicting blood pressure without cuff than the features extracted manually from other studies.

3.3.4 Performance comparison

Table 3.2 shows the comparison of BP prediction accuracy between the proposed method and previous studies. Most studies used mean absolute error (MAE) as an evaluation metric of BP prediction accuracy, and we also compared the results using MAE.

Training without consideration of train/test data split by subject would result in an abnormally high BP prediction accuracy because the subject data used in the training phase may be used in the test phase. For a fair comparison, we did not compare the performance with the results of studies not considering train/test data split by subject [66], [33], [70], [19] and the study using private dataset [66]. We compared only the results obtained under the same conditions in this study.

From the results in Table 3.2, we can confirm that both the calibration-free and calibration-based BP prediction methods in this study show the best performance compared with other studies. In calibration-free settings, the performances of both

Table 3.2: Comparison of BP prediction accuracy with other related works

	Dataset	Author	Input	Model	Input	SBP(mmHg)		DBP(mmHg)	
						MAE	STD	MAE	STD
Cal-free	MIMIC II	M. Kachuee[31]	Features	ML ensemble	ECG, PPG	11.17	10.09	5.35	6.14
	MIMIC II	Ours	Raw	CNN	ECG, PPG	**9.30**	8.85	**5.12**	5.52
	Queensland	Y. Zhang[78]	Features	SVM	PPG	11.64	8.20	7.62	6.78
	MIMIC II	Ours	Raw	CNN	PPG	**10.86**	9.54	**5.95**	5.60
Cal-based	MIMIC II	M. Kachuee[31]	Features	ML ensemble	ECG, PPG	8.21	5.45	4.31	3.52
	MIMIC II	Ours	Raw	CNN	ECG, PPG	**5.32**	5.54	**3.38**	3.82
Without train/test data split by subject†	Self-made	P. Su‡[66]	Features	LSTM	ECG, PPG	3.73‡		2.43‡	
	MIMIC II	O. F. Ertugrul[19]	Features	ELM	ECG, PPG	4.37		3.95	
	Queensland	S. Khalid[33]	Features	Regression tree	PPG	4.82	4.31	3.25	4.17
	MIMIC II	L. Wang[70]	Features	ANN	PPG	4.02	2.79	2.27	1.82
	MIMIC II	O. F. Ertugrul[19]	Features	ELM	PPG	4.25		3.95	

† Training without consideration of train/test data split by subject would result in an abnormally high BP prediction accuracy because the subject data used in the training phase may be used in the test phase.

‡ Root-mean-square-error (RMSE)

ECG+PPG and PPG only improve significantly compared with previous studies: SBP 16.7% (11.17→9.30) and DBP 4.3% (5.35→5.12) with ECG+PPG, SBP 6.7% (11.64→10.86) and DBP 21.9% (7.62→5.95) with PPG only. These results show that the proposed CNN method can work flexibly with various input combinations. An in-depth analysis of this will be described in chapter 3.3.6. Notably, It is encouraging that the improvement with calibration is much more substantial (SBP 35.2%, DBP 21.6%) than the result without calibration. This is due to the strong approximation performance of CNN compared to other machine learning methods. From an application perspective, we can expect that the proposed method will be robust with a wearable device, which requires personalized calibration.

3.3.5 Verification using international standards for BP measurement grading criteria

Association for the Advancement of Medical Instrumentation (AAMI)

Table 3.3 presents the verification results of the proposed method using CNN based estimation model with the AAMI standard. The criteria for fulfilling the AAMI protocol are that the test device must not differ from the mercury standard by a mean error (ME) of $\leq$5 mmHg or a standard deviation (STD) of $\leq$8 mmHg. According

Table 3.3: Verification with the AAMI Standard

			Diffrence between standard and predicted value(mmHg)		
			ME	STD	Subjects
Proposed	Cal-free	DBP	0.13	7.54	379
		SBP	-1.23	12.80	
	Cal-based	DBP	-0.48	5.08	
		SBP	-1.29	7.58	
AAMI		SBP/DBP	≤ 5	≤ 8	$\geq$85

to the AAMI grading criteria, almost all of the calibration-free and calibration-based methods proposed in this study satisfy the AAMI criteria for both BSP and DBP. The standard deviation value of the SBP is slightly over the AAMI standard limit[51].

British Hypertension Society (BHS)

Table 3.4 presents the verification results of the proposed method using CNN based estimation model with the BHS standard. The BHS grading criteria represent the cumulative percentage of readings falling within 5 mmHg, 10 mmHg, and 15 mmHg of the mercury standard. All three percentages must be greater than or equal to the values shown for a specific grade to be awarded. The criteria for fulfilling the BHS protocol are that devices must achieve at least grade B (where A denotes the greatest agreement with mercury standard and D denotes least agreement) for systolic and for diastolic pressures. Mean arterial pressure (MAP) is defined as the average pressure in a patient's arteries during one cardiac cycle. It can be calculated from the SBP and

Table 3.4: Verification with the BHS Standard

			Absolute difference			Grade
			≤ 5	≤ 10	≤ 15	
Proposed	Cal-free	DBP	64.1%	87.1%	95.0%	A
		SBP	40.6%	67.5%	80.2%	D
		MAP	62.0%	87.1%	95.8%	A
	Cal-based	DBP	79.2%	95.3%	97.9%	A
		SBP	59.6%	87.3%	93.7%	B
		MAP	79.7%	96.0%	99.2%	A
BHS		grade A	60%	85%	95%	
		grade B	50%	75%	90%	
		grade C	40%	65%	85%	

the DBP using the formula [13]:

$$MAP = \frac{SBP + 2(DBP)}{3} \tag{3.4}$$

According to the BHS grading criteria, the proposed calibration-free method achieved A grade in the prediction of DBP and B grade in the prediction of MAP value. In the case of calibration-free method, for SBP, the proposed method achieved a grade lower than B. After considering the calibration-based method actually in use the proposed method achieved an A grade in DBP and a B grade in SBP predictions. The proposed method satisfies the BHS standard completely except for SBP in the case of calibration-free method [51].

3.3.6 Performance comparison by the input signal combinations

The concept of estimating BP using a single biomedical signal such as PPG or ECG that can be easily measured from a mobile device such as a smartphone or a watch seems to be promising. The same experiment was conducted using a single PPG or ECG signal as the input for the development of the wearable product.

Table 3.5 presents the accuracy of the experiment for different input signal combinations. The accuracy is the best when both the time and frequency encoders of PPG+ECG inputs are used. In the case of using a single ECG or PPG signal, the BP prediction performance is lower than the case of using both input signals together. However, as shown in Table 3.2, this result shows superior BP prediction performance compared with other previous experiments using the same input signal. In all three cases using ECG+PPG, PPG, and ECG as inputs, it can be seen that the accuracy is higher when time and frequency signals are used together than when only a time or a frequency signal is used. The performance improvement due to the corre-

Table 3.5: Performance comparison by the input signal combinations

		Cal-free				Cal-based			
		SBP		DBP		SBP		DBP	
		MAE	STD	MAE	STD	MAE	STD	MAE	STD
Time + Freq.	PPG+ECG	**9.30**	8.85	**5.12**	5.52	**5.32**	5.54	**3.38**	3.82
	PPG only	10.86	9.54	5.95	5.60	7.16	6.79	4.48	4.60
	ECG only	11.46	9.73	5.72	5.55	7.29	6.87	4.39	4.49
Time only	PPG+ECG	10.13	9.48	5.45	5.34	5.93	6.13	3.63	3.83
	PPG only	11.15	9.82	5.71	5.98	7.41	7.02	4.32	4.50
	ECG only	11.57	10.78	5.81	6.00	7.00	6.82	4.14	4.43
Freq. only	PPG+ECG	11.66	10.65	5.95	5.60	9.49	9.14	5.02	5.04
	PPG only	12.43	11.43	6.17	6.14	11.25	10.15	5.85	5.53
	ECG only	11.79	10.30	5.70	5.61	9.33	8.62	4.92	4.55

lation is larger when the time signal is used than the frequency signal. In addition, PPG signal does not seem to be helpful for learning when only frequency domain of PPG signal is used. To verify this result, an ablation experiment was conducted using the input combination where only the frequency encoder of PPG is removed from the best combination (both the time and frequency encoders of PPG+ECG inputs are used). The accuracy of BP prediction was found to be SBP 9.60 ± 9.53 and DBP 5.14 ± 5.10 for calibration-free, and SBP 5.98 ± 6.17 and DBP 3.81 ± 3.96 for calibration-based, respectively. This result is worse than those of the best combination. This result shows that any relation between time and frequency input contributes to the improvement of BP prediction performance. Our proposed model can learn this relationship to improve accuracy.

3.3.7 An ablation study of each architectural component of extraction-concentration blocks

The ablation experiment was conducted using both the time and frequency encoders of PPG+ECG signals together as inputs, to verify the effectiveness of each architectural component on the final accuracy. To verify the effectiveness of each architectural component, we conducted three types of experiment. First, we directly excluded the residual connection inside the *Extraction block* to observe the network performance. Second, we directly excluded the *Extraction block*. Third, we conducted the experiment without the *Concentration block*. However, if the *Concentration block* is removed entirely, down-sampling will not be possible. Hence, we switched the *Concentration block* to the maxpool layer instead of directly excluding the *Concentration block*.

Table 3.6 presents the accuracy of the experiment excluding each architectural component. When the *Extraction block* is removed altogether, the drop-in accuracy is greater than when only the residual connection inside the *Extraction block* is removed. The proposed model can learn the various relationships between different neighboring pixels through the *Extraction block*, which is concatenated with each output of multiple dilated convolutions, simultaneously. Furthermore, the use

Table 3.6: Performance comparison by excluding architectural components of extraction-concentration blocks

	Cal-free			
	SBP		DBP	
	MAE	STD	MAE	STD
Final model	**9.30**	8.85	**5.12**	5.52
w/o residual connection	9.87	9.41	5.69	6.61
w/o extraction block	10.47	9.88	6.19	6.86
w/o concentration block	11.51	10.35	6.42	7.22

of strided convolution with a large kernel inside the *Concentration block* has the greatest effect on accuracy improvement. This result shows that considering a wide range of multiple pixels together in the down-sampling step through strided convolution with a large kernel size, instead of pooling in the *Concentration block*, has a significant effect on the improvement of accuracy.

3.3.8 Preprocessing of input signal to improve blood pressure prediction performance

In order to improve the final performance of the blood pressure prediction model created through several experiments previously, preprocessing of the input signal was performed. First, for frequency domain input, we increase the frequency input depth by concatenating the input signal's phase term. Next, normalization was performed on the training dataset, and the values in the distribution were shifted to the standard deviation unit and displayed again. It can be calculated using the formula:

$$x = \frac{x - m}{\sigma}(m : average, \sigma : standard\ deviation) \tag{3.5}$$

Third, we exclude abnormal input signals through peak analysis, with the peak constraints defined as $\mathrm{len}(p) \geq 5, \mathrm{StdVar}(\Delta p_x) < 5, \mathrm{StdVar}(p_y) < 5$, where peak $p = (p^1, .., p^n)$, p_x^i is the time stamp and p_y^i is the input value of the ith peak. After detecting the peak of PPG, signal alignment was performed so that the signal starting from the peak of PPG can be used for training. Table 3.7 presents the accuracy of the BP prediction model after performing the input preprocessing. The performances of input signal preprocessing improve compared with previous studies: SBP 2.4% (9.30→9.08) and DBP 0.8% (5.12→5.08) with phase term, SBP 2.9% (9.30→9.03) and DBP 1.2% (5.12→5.06) with normalization, SBP 7.6% (9.30→8.59) and DBP

Table 3.7: Performance comparison by performing input signal preprocessing

	Cal-free			
	SBP		DBP	
	MAE	STD	MAE	STD
Final model	9.30	8.85	5.12	5.52
w/ phase	9.08	8.79	5.08	5.38
w/ normalization	9.03	8.71	5.06	5.38
w/ constraint	8.59	8.31	4.90	4.82
w/ all preprocessing	**8.41**	8.12	**4.83**	4.81

4.3% (5.12→4.90) with constraint, SBP 9.6% (9.30→8.41) and DBP 5.7% (5.12→4.83) with all preprocessing. These results show that increasing the frequency input depth by connecting the phase of the input signal and rescaling the input signal through normalization helps a little in training the model. Furthermore, it is considered that removing the abnormal input signal through constraints and conducting the training is very helpful in improving the performance of the BP prediction model.

3.4 Discussion

In this paper, we designed the filter size to consider wide range which is different from the general filter structure ($k = 3$) used mainly in the field of vision. We believe that the large receptive field due to the wide filter size is more effective in solving the regression problem of the sequential signal than the small receptive field of the general CNN structure. In particular, a multi-dilated convolution based extraction block designed to consider various values (when $k = 7$, 7$\sim$25 pixels around, up to 0.2 seconds) based on a reference pixel has played an important role in improving BP prediction accuracy.

The proposed method can be easily applied to an on-device application for several reasons: 1) It is possible to train and predict BP values using a short time duration (about 8 seconds); 2) It is possible to combine various inputs such as ECG and/or PPG signals to utilize the measurable biomedical signal according to the conditions of the device; 3) It uses the raw signal as input without unique feature extraction. Notably, an on-device application has the advantage that there is no need for additional equipment or special conditions (synchronization, etc.) for feature extraction.

We applied two constraints to the ABP signal, which is the target value of prediction as a minimum refinement for proper training. No constraints were applied to ECG and PPG used as inputs to training. In other words, we did not exclude any abnormal inputs for training, which allowed us to create a model that is robust to signal measurement errors and noise.

The MIMIC II database used in this paper has several potential limitations on performance improvements: 1) Sampling rate of MIMIC II database is very low for today's minimum recommended 1000 Hz sampling rate [35]. It is expected that the performance improvement will be possible when using data with a higher sampling

rate. However, it should be verified whether the proposed model structure and data preprocessing method are still valid. If necessary, it would be possible to propose a new model structure that is effective for high sampling rate data through further studies. 2) It was obtained from intensive care units (ICU), which means that the average age and BP value of subjects are higher than average age and BP value of the total population. We will conduct experiments using large amounts of unbiased data through consultation with medical experts to improve performance.

We propose fully convolutional networks constructed using only 1D convolution for BP prediction. Based on the architecture of CNN, our method has a flexibility to deal with input variations and can predict BP without much consideration of the relationship with previous sequence. Future work will include a detailed inspection of other possible deep architectures for potentially improving the initial results with CNN. From a wearable application perspective, it is essential to calibrate the pre-trained model to fit each individual. In this study, we show that the BP prediction performance of the model is improved through basic calibration using a public dataset. It will become more necessary to study precise calibration technology which is more personalized. Future research will focus on improving personalized BP prediction performance by using private data on the pre-trained model using a public dataset.

3.5 Summary

In this paper, we have developed a calibration-free, cuffless BP prediction method based on the deep CNN model. BP measurement is important in monitoring health conditions to prevent heart disease and stroke. In this method, we can predict BP using ECG and PPG signals that can be easily measured through various sensors without the inconvenience of wearing cuffs. Unlike many previous studies, we have shown that BP can be estimated better than in previous studies by directly using raw signals without any unnecessary preprocessing procedure to extract features from ECG and PPG signals. The performance of this model was verified by comparing with the accuracy of other researchers' previous studies and various international standards for BP measurement grading criteria. Through comparison with international standards, we confirmed that BP prediction accuracy of the method proposed in this paper is sufficiently high to recommend for clinical use.

Chapter 4

Blood pressure prediction by a smartphone sensor using fully convolutional networks

Heart disease and stroke are the leading causes of death worldwide. High blood pressure greatly increases the risk of heart disease and stroke. Therefore, it is important to control blood pressure (BP) through regular BP monitoring; as such, it is necessary to develop a method to accurately and conveniently predict BP in a variety of settings. In this paper, we propose a method for predicting BP without feature extraction using fully convolutional neural networks (CNNs). We measured single multi-wave photoplethysmography (PPG) signals using a smartphone. To find an effective wavelength of PPG signals for the generation of accurate BP measurements, we investigated the BP prediction performance by changing the combinations of the input PPG signals. Our CNN-based BP predictor yielded the best performance metrics when a green PPG time signal was used in combination with an instantaneous frequency signal. This combination had an overall mean absolute error (MAE) of 5.28 and 4.92 mmHg

for systolic and diastolic BP, respectively. Thus, our CNN-based approach achieved comparable results to other approaches that use a single PPG signal.

4.1 Introduction

High blood pressure, clinically referred to as hypertension, is known as a "silent killer" due to its inconspicuous symptoms and potentially life-threatening complications. It is therefore important for individuals to control their blood pressure (BP) through regular BP measurements. However, BP may increase or decrease temporarily depending on an individual's situation, such as their location and the time of day when BP is measured. "Masked hypertension" occurs when the individual's BP is actually high but is measured as normal in a doctor's office. This phenomenon is present in approximately 10% of normal adults and may cause more damage to the heart or other organs than clinically detected normal, thus requiring more thorough BP control [54]. Conversely, "white coat hypertension" occurs when the patient is nervous when seeing a doctor and therefore their BP increases despite their actual BP being normal. This phenomenon is reported to occur in approximately 15% of the general population and in approximately one-third of patients diagnosed with hypertension [23]. Medication should be given to patients with white coat hypertension who also have damage to organs such as the heart, brain, and kidneys and those who are at high risk for cardiovascular disease. Therefore, in order to make an accurate diagnosis, it is important to self-measure BP periodically in a relaxed state in addition to regularly having BP measurements performed by a medical professional in a clinical setting. Periodic self-measurement of BP is highly reproducible and provides clinically important information in the diagnosis and treatment of hypertension, which is very useful for long-term BP management. Furthermore, self-measurement is beneficial for the evaluation of BP changes over time, and reduces the inconvenience and cost of regular visits to medical institutions for monitoring.

Despite the many advantages of self-measurement of BP, the conventional com-

mercially available autonomous BP measuring devices are difficult to carry and use outside the home, and are challenging to use during walking. Therefore, it is necessary to develop a method for accurate, comfortable and convenient BP self-measurement that can be used in a variety of settings. Recently, various studies have been conducted regarding the prediction of BP through single photoplethysmography (PPG) signals measured by one PPG sensor [78, 27, 33, 38, 58]. In addition, multi-wavelength PPG detection technology has been shown to be superior to single-wavelength PPG, and it has been considered a powerful method for measuring PPG signals [4]. It has also been noted that PPG sensing light sources of different wavelengths are recommended for different skin tones [75]. Previous studies on BP prediction using PPG signals generally consist of feature extraction followed by machine learning or regression-based prediction. A variety of combinations of PPG signal features, including time-domain, frequency-domain, and entropy-based features, among others, have been used to date as key features for BP prediction. Recently, in BP prediction research using electrocardiography (ECG) in conjunction with PPG signals, an end-to-end approach with self-generated features using deep-learning technology has been used [68, 1].

In this paper, we propose a method for predicting BP without feature extraction using only PPG signals measured by smartphone using the convolutional neural networks (CNN) model proposed in the previous study [1]. Instead of using additional physiological cardiovascular signals, multiple wavelengths of PPG (infrared, red, green, blue) signals were measured using the smartphone's heart rate monitor sensor and analyzed to determine the optimal combination of PPG signals for predicting systolic BP (SBP) and diastolic BP (DBP). The main contributions of our work are summarized as follows:

- We proposed a novel end-to-end method of predicting BP using only a single

PPG signal without manual feature extraction.

- We optimized BP prediction performance by testing various combinations of PPG signal wavelengths to maximize prediction accuracy.
- Our CNN-based approach achieved comparable results to other approaches that require a single PPG signal.

4.2 Method

The BP prediction process involved acquiring multiple wavelengths of PPG signals from a smartphone, PPG signal preprocessing, data preparation, and BP predictions using a CNN-based prediction model. A schematic of the methodology is depicted in Fig. 4.1.

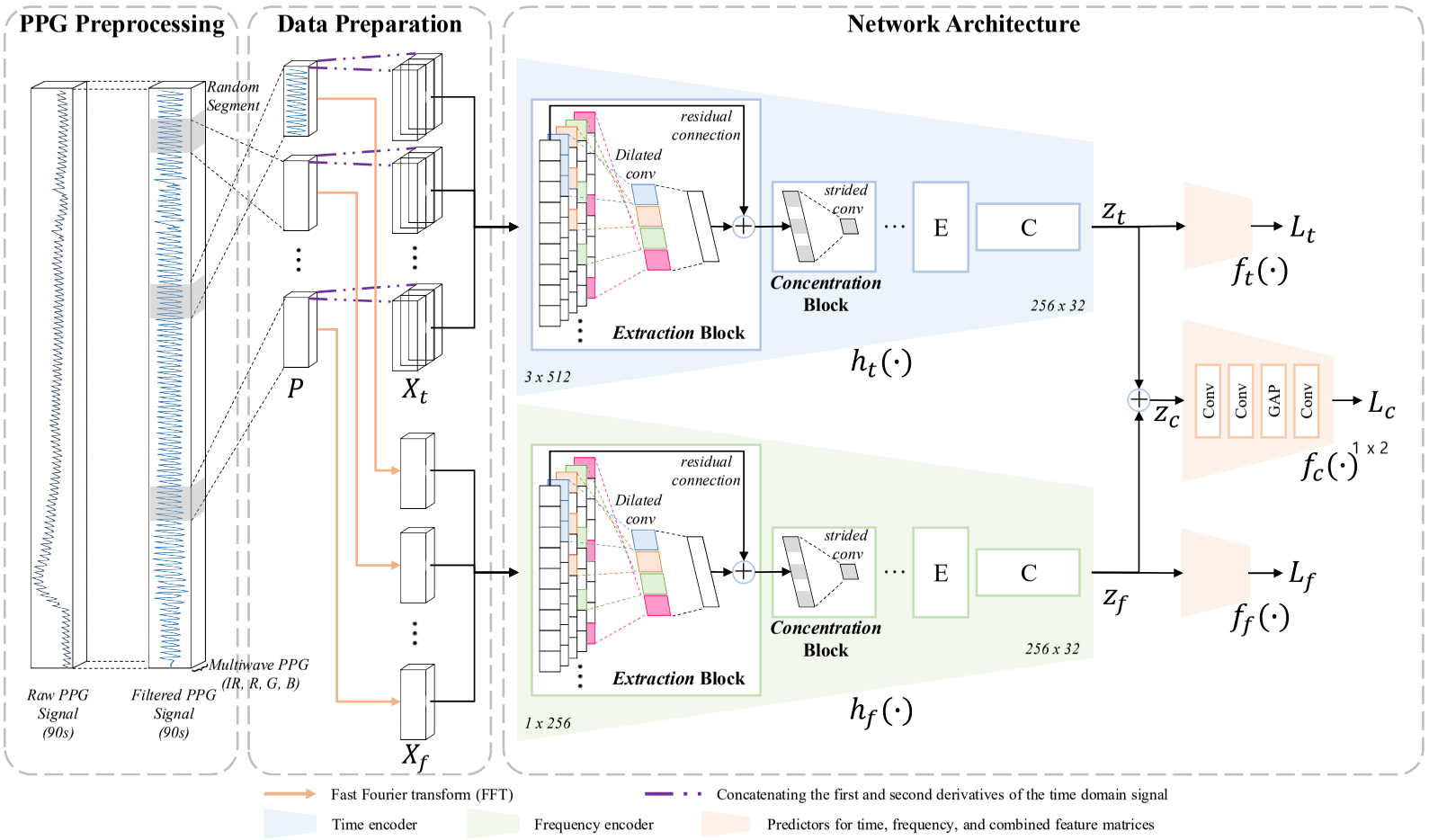

Figure 4.1: Overview of the BP prediction methodology.

4.2.1 Data acquisition

PPG data were acquired using the heart rate sensor of the Samsung Galaxy Note8 smartphone. The sampling frequency was 100 Hz and four multi-wavelength PPG signals were used: infrared (IR), red (R), green (G), and blue (B). The data was collected from 26 volunteers. In all experiments, informed consent was obtained from all subjects and the data were used anonymously only for the intended research purpose. Also, the principles outlined in the Helsinki Declaration were followed. The PPG data was collected 23 times in 90 s length under various conditions including resting, exercising and sleeping. In the resting condition, the subject was seated and the reference BP measurement and PPG signal gathering was performed simultaneously in 2 minute intervals. During the exercise condition—which was intended to induce an increase in BP—the subject performed the leg press exercise with a weight in the range of 5 to 40 kg depending on their exercise abilities. After the exercise session, the subject was asked to sleep for 2 hours to decrease their BP. For the reference BP reading, two trained nurses measured BP simultaneously using the auscultatory method. The nurses' values for each reference reading were averaged unless the values had a difference of greater than 4 mmHg.

4.2.2 Preprocessing of the PPG signals

The PPG signal was first resampled at a sampling rate of 250 Hz and detrended to remove direct current components. Next, a bandpass filter with a passband of 0.4-8 Hz was applied to separate out the noise components.

4.2.3 PPG signal selection

To investigate the influence of the four multi-wavelength PPG signals on the performance of the BP prediction method, we investigated 15 PPG signal combinations

as follows: IR, R, G, B, IR+R, IR+G, IR+B, R+G, R+B, G+B, IR+R+G, IR+R+B, IR+G+B, R+G+B, IR+R+G+B.

4.2.4 Data preparation for CNN model training

The dataset contained a set of 90 s of raw IR, red, green, blue PPG signal data in the form $P_i = (p_i^{\mathrm{IR}}, p_i^{\mathrm{Red}}, p_i^{\mathrm{Green}}, p_i^{\mathrm{Blue}})$, with SBP and DBP values denoted by $Y_i = (y_i^{\mathrm{SBP}}, y_i^{\mathrm{DBP}})$, where i is the subject index. The PPG signal data was separated into training (60 s), validation (10 s), and test (20 s) datasets. The data was prepared as input and output data pairs (x,y) suitable for CNN model training. Three data preparation techniques were used: random cropping, increasing input depth using its derivatives, and fast Fourier transform (FFT). Random cropping allows the model to learn signals from multiple points of input. Since our model required both time and frequency components as input signals, we concatenated the first and second derivatives of the time-domain signal to the original time-domain signal to increase the depth of the input signal as follows [37]:

$$X_t = X_t \oplus \Delta X_t \oplus \Delta^2 X_t \tag{4.1}$$

Finally, we converted the original time-domain signal to a frequency-domain signal using FFT. Thus, the dataset (X_t, X_f, Y) was prepared for CNN model training.

4.2.5 Network architectures

To learn the frequency characteristics as well as time features from the original PPG, we proposed a CNN-based BP prediction model. It consists of three parts: a time encoder, a frequency encoder, and three predictors for time, frequency, and combined feature matrices. The time encoder $h_t(\cdot)$ learns representative features from

time-series inputs x_t, and outputs the corresponding feature matrix z_t. In parallel with the time encoder, the frequency encoder $h_f(\cdot)$ outputs the feature matrix z_f for the frequency domain inputs, x_f. Each encoder is composed of two stacked core modules named the *extraction* and *concentration blocks*, which are designed to effectively learn latent features from the periodic data. The *extraction block* can learn the various relationships between different neighboring pixels through multiple dilated convolutions, whereas the *concentration block* can consider a wide range of multiple pixels together in the down-sampling step through strided convolution. Both the time encoder and the frequency encoder consist of four *extraction+concentration* combinations. After feature extraction through both the time and frequency encoders, the combined feature matrix $z_c = z_t \oplus z_f$ can be defined. The combined predictor $f_c(\cdot)$ consists of a double stacked convolution layer, global average pooling, and a dimension reduction convolution layer. The output $\hat{y_c}$ of $f_c(\cdot)$ is two real numbers which indicate SBP and DBP. The prediction minimizes the distance between the target y and the prediction y_c. The minimization objective is defined as

$$L_c = d(y_c, \hat{y_c}), \tag{4.2}$$

where d can be any distance metric between real numbers; in this case, L1. In addition to this, two auxiliary flows from the predictors $f_t(\cdot)$ and $f_f(\cdot)$ were added which take the pre-concatenated features z_t and z_f as inputs, respectively. Both auxiliary predictors have a simpler structure which consists of one convolution layer, global average pooling, and a dimension reduction convolution layer. Auxiliary loss is a well-known technique to help the model's gradient flow in the back-propagation phase and improve performance. We introduce the importance factor α to both losses L_t and L_f.

Our final loss is then defined as follows:

$$L_{\text{total}} = L_c + \alpha(L_t + L_f), \tag{4.3}$$

where the weight of auxiliary loss α = 0.2, in this case.

4.3 Experimental results

4.3.1 Implementation details

The CNN-based model was implemented in Python with Pytorch [52] based on a deep learning framework, which was trained with a maximum of 50 epochs. The Adam optimizer with $\beta_1 = 0.9,\ \beta_2 = 0.999$, and no weight decay was used. The initial learning rate was 0.0001 and the dropout rate was set to 0.2 for the entire network. In this study, the model was run on a machine with six central processing units (CPUs; Intel i7-6850K CPU @ 3.6GHz) on an Ubuntu 16.04 platform. Four graphic processing units (GPUs; NVIDIA RTX 2080 Ti) were also used to accelerate the processing of the experiments.

4.3.2 Effect of PPG combination on BP prediction

Evaluations on the different input combinations of PPG signals for the CNN were conducted. The model was trained using only the selected PPG signals according to the specified input combination. Table 4.1 shows the BP prediction accuracy of the CNN-based BP prediction for different input PPG signal combinations. As shown in Table 4.1, using only the green signal as an input yielded the best performance on average compared to other input signal combinations. This indicates that the green PPG signal has the most required information for accurate BP prediction. In most subjects, the highest accuracy was achieved with the green PPG signal only as an input, but higher accuracy was observed for some subjects with a blue signal as input. Reflecting the most accurate results for each subject, the BP prediction errors are SBP 4.47 and DBP 4.03, which are 15.3% and 18.1% better than the green signal alone as an input, respectively.

Table 4.1: BP prediction performance by the input PPG combinations

	SBP		DBP	
	MAE†	STD‡	MAE	STD
Infrared	5.69	1.64	5.02	1.79
Red	6.24	2.40	5.74	2.98
Green	**5.28**	1.80	**4.92**	2.42
Blue	5.53	1.77	4.92	2.05
Infrared+Red	6.02	1.91	5.42	2.25
Infrared+Green	5.92	2.49	5.32	2.04
Infrared+Blue	5.67	2.20	5.36	2.51
Red+Green	5.38	1.73	5.10	2.16
Red+Blue	5.56	1.86	5.29	2.93
Green+Blue	5.56	2.06	5.44	2.46
Infrared+Red+Green	6.03	4.17	5.58	2.66
Infrared+Red+Blue	5.78	2.27	5.63	2.49
Infrared+Green+Blue	5.81	2.13	5.34	2.54
Red+Green+Blue	5.68	1.80	5.21	2.38
Infrared+Red+Green+Blue	5.32	1.49	5.32	2.49

† MAE = mean absolute error, ‡ STD = standard deviation

4.3.3 Performance comparison with other related works

Table 4.2 shows the comparison of BP prediction accuracy between the proposed method and previous studies. From Table 4.2, it can be seen that the CNN-based BP prediction method in this study showed comparable performance to other studies using a single PPG signal. In addition, it can be seen that the performance are equivalent when compared with the end-to-end BP prediction study using both ECG and PPG. From an application perspective, we can expect that the proposed method will be robust for a wearable device, which limits the use of multiple sensors.

Table 4.2: Comparison of BP prediction accuracy to other works

	SBP		DBP	
	MAE	STD	MAE	STD
Y. Zhang [78]	11.64	8.20	7.62	6.78
S. Khalid [33]	4.82	4.31	3.25	4.17
M. Radha† [58]	7.86	1.57	6.49	1.59
S. Baek‡ [1]	5.32	5.54	3.38	3.82
Ours (Green)	5.28	1.80	4.92	2.42
Ours (Best)	4.47	1.53	4.03	1.48

† Root-mean-square-error (RMSE)
‡ End-to-end BP prediction using ECG, PPG

4.3.4 Verification using international standards for BP measurement grading criteria

Association for the Advancement of Medical Instrumentation (AAMI)

Table 4.3 presents the verification results of the proposed method using CNN based estimation model with the AAMI standard. The criteria for fulfilling the AAMI protocol are that the test device must not differ from the mercury standard by a mean error (ME) of $\leq$5 mmHg or a standard deviation (STD) of $\leq$8 mmHg. According to the AAMI grading criteria, our method proposed in this study satisfy the AAMI criteria for both BSP and DBP[51].

Table 4.3: Verification with the AAMI Standard

		Diffrence between standard and predicted value(mmHg)		
		ME	STD	Subjects
Ours	DBP	1.34	7.12	90
	SBP	1.47	6.42	
AAMI	SBP/DBP	≤ 5	≤ 8	$\geq$85

British Hypertension Society (BHS)

Table 4.4 presents the verification results of the proposed method using CNN based estimation model with the BHS standard. The BHS grading criteria represent the cumulative percentage of readings falling within 5 mmHg, 10 mmHg, and 15 mmHg of the mercury standard. All three percentages must be greater than or equal to the values shown for a specific grade to be awarded. The criteria for fulfilling the BHS protocol are that devices must achieve at least grade B (where A denotes the greatest agreement with mercury standard and D denotes least agreement) for systolic and for diastolic pressures. Mean arterial pressure (MAP) is defined as the average pressure in a patient's arteries during one cardiac cycle. It can be calculated from the SBP and the DBP using the formula [13]:

$$MAP = \frac{SBP + 2(DBP)}{3} \tag{4.4}$$

According to the BHS grading criteria, the proposed method achieved C grade in the prediction of DBP, A grade in the prediction of SBP and B grade in the prediction of MAP value. The proposed method satisfies the BHS standard completely except for DBP [51].

Table 4.4: Verification with the BHS Standard

		Absolute difference			Grade
		≤ 5	≤ 10	≤ 15	
Ours	DBP	49.6%	82.1%	94.5%	C
	SBP	62.4%	86.9%	95.3%	A
	MAP	52.2%	78.7%	91.8%	B
BHS	grade A	60%	85%	95%	
	grade B	50%	75%	90%	
	grade C	40%	65%	85%	

4.3.5 Preprocessing of input signal to improve blood pressure prediction performance

In order to improve the final performance of the blood pressure prediction model created through several experiments previously, several preprocessing of the input signal was performed. First, for frequency domain input, we increase the frequency input depth by concatenating the input signal's phase term. Next, normalization was performed on the training dataset, and the values in the distribution were shifted to the standard deviation unit and displayed again. It can be calculated using the formula:

$$x = \frac{x - m}{\sigma}(m : average, \sigma : standard\ deviation) \tag{4.5}$$

Third, we exclude abnormal input signals through peak analysis, with the peak constraints defined as $\mathrm{len}(p) \geq 5, \mathrm{StdVar}(\Delta p_x) < 5, \mathrm{StdVar}(p_y) < 5$, where peak $p = (p^1, .., p^n)$, p_x^i is the time stamp and p_y^i is the input value of the ith peak. After detecting the peak of PPG, signal alignment was performed so that the signal starting from the peak of PPG can be used for training. Table 4.5 presents the accuracy of the BP prediction model after performing the input preprocessing. The performances of input signal preprocessing improve compared with previous studies: SBP 0.4%

Table 4.5: Performance comparison by performing input signal preprocessing

	SBP		DBP	
	MAE	STD	MAE	STD
Ours (Green)	5.28	1.80	4.92	2.42
w/ phase	5.26	1.78	4.93	2.42
w/ normalization	5.07	1.82	4.80	2.37
w/ constraint	4.82	1.73	4.61	2.29
w/ all preprocessing	**4.74**	1.69	**4.53**	2.21

(5.28→5.26) and DBP -0.2% (4.92→4.93) with phase term, SBP 4.0% (5.28→5.07) and DBP 2.4% (4.92→4.80) with normalization, SBP 8.7% (5.28→4.82) and DBP 6.3% (4.92→4.61) with constraint, SBP 10.2% (5.28→4.74) and DBP 7.9% (4.92→4.53) with all preprocessing. These results show that rescaling the input signal through normalization helps to train the model. Furthermore, it is considered that removing the abnormal input signal through constraints and conducting the training is very helpful in improving the performance of the BP prediction model.

4.4 Discussion

Our CNN-based BP prediction method achieved the best performance in most cases using a green PPG time signal in combination with an instantaneous frequency signal. It used the raw PPG signal as an input without unique feature extraction. Notably, an on-device application is advantageous as there is no need for additional equipment or special conditions for feature extraction. Interestingly, some subjects had greater BP prediction accuracy with the blue PPG signal as the input. In BP estimation, a red or IR PPG light is often used because the long wavelength is able to penetrate deeper into the skin and is more capable of detecting signals from the deep arteries [60]. However, since the light also travels through the epidermis and dermis, the variation in the detected light is a complex result of the concurrent changes in the volume of the arteries, arterioles, capillaries, and veins. In other words, signals such as green and blue, which have low skin penetration depth, have information that is most relevant to predicting BP. Since the amount of data used in the experiment was small and no additional information such as skin color was identified, the explanation of the improved accuracy of the blue PPG signal for some subjects cannot be confirmed, but it is possible that this effect was due to variations in skin tone. Of course, the accuracy of blood pressure prediction of methods using time delays such as PTT and PAT is very high. However, in order to obtain this time delay, ECG and PPG should be measured simultaneously or PPG at two points. Since it is difficult to know this time delay in terms of measuring blood pressure comfortably through a wearable device, it is very important to predict the blood pressure by analyzing signals such as PPG and ECG itself. With deep learning, various features of the signal itself can be well extracted, making it possible to accurately predict blood pressure values without the inconvenience of finding appropriate features. This method can be useful for patients

who do not tolerate traditional blood pressure monitoring because the cuff is not used and there is less interference to the patient. It can also be especially useful in cases where an evaluation that does not interfere with sleep is important, such as breathing disorders, as it does not interfere with the patient's sleep when measuring blood pressure. Future research will focus on improving personalized BP prediction performance by using PPG light combinations tailored for each individual.

4.5 Summary

In this paper, we proposed a method for predicting BP without feature extraction using a single PPG signal measured by smartphone using fully convolutional networks. The concept of estimating BP using a single biomedical signal such as PPG that can be easily measured from a mobile device without the inconvenience of wearing a cuff is promising for self-monitoring of BP. Unlike many previous studies, we have shown that BP can be estimated directly from raw signals without preprocessing to extract features from the PPG signal. Our study was limited given that data acquisition was from only 26 volunteers and no other additional information such as skin color was recorded. We plan to expand our research, including by acquiring data that can be verified by IEEE Standard 1708-2014, a universal standard for the validation of BP measuring devices.

Chapter 5

Improving accuracy of blood pressure prediction by distilling the knowledge of neural networks

This paper proposes a method to improve the accuracy of predicting blood pressure by using only photoplethysmogram. Specifically, the proposed approach distills the training knowledge of the teacher model, which predicts the BP using both photoplethysmogram and electrocardiogram, into a student model, which predicts the BP using only photoplethysmogram, while simultaneously training the two models. The accuracy of the model using only photoplethysmogram to predict the systolic and diastolic blood pressure was improved by 5.4% and 10.4%, respectively, compared to the accuracy before using the knowledge distillation process.

5.1 Introduction

Hypertension is a condition in which the pressure of blood flowing through blood vessels, that is, the blood pressure (BP) level continuously indicates a systolic of 140 mmHg or diastolic or more than 90 mmHg. Hypertension itself is not scary, but long-term neglect that it may be a severe hypertensive patient can lead to many life-threatening complications. In order to prevent such complications, regular blood pressure (BP) measurement is very important, and research is being conducted on ways to easily measure BP without cuff. These studies predict BP by analyzing the relationship between bio signals, such as ECG and PPG, or the characteristics of each signal itself. In general, it is known that the combination of ECG and PPG shows higher BP prediction accuracy than that of the PPG signal alone[1]. The BP is applied to the blood vessels by the heartbeat generated by the heart's special excitement conduction system, which causes blood flow in the blood vessels and blood flow to the peripheral blood vessels. At this time, the signal represented by the vector sum of the action potentials of the heart is the ECG, and the signal that measures the blood flow of the peripheral blood vessels through the optical sensor is PPG. While measuring ECG requires 4 to 12 electrodes, PPG is much easier to measure using only LEDs and photosensors. In this paper, we suggest the structure that improve the ability to predict BP using only PPG by distilling well-trained knowledge of the teacher model into a student model while simultaneously training two models, a teacher model that predicts BP using PPG and ECG, and a student model that predicts BP using PPG. Through the knowledge distillation (KD), the knowledge of the teacher model that learned from ECG and PPG together is transferred to the student model that is trained with only the PPG, thereby improving the BP prediction performance of the student model. In addition, it has the advantage of being able to inference with PPG without

ECG while showing high performance. Although hypertension itself is not a critical condition, long-term neglect in a patient with severe hypertension may lead to many life-threatening complications. To prevent such complications, the blood pressure (BP) must be regularly monitored, and extensive research is being performed to easily measure the BP without using cuffs. In general, the BP is predicted by analyzing the relationship between the bio signals, such as electrocardiogram (ECG) and photoplethysmogram (PPG), or the characteristics of each signal. Using both the ECG and PPG to predict the BP leads to a higher prediction accuracy than that when using only the PPG signal [1]. However, measuring the ECG requires 4–12 electrodes, whereas PPG can be easily measured using only LEDs and photosensors. Considering these aspects, this paper proposes a structure to improve the BP prediction accuracy when using only the PPG. Specifically, the proposed approach distills the training knowledge of the teacher model, which predicts the BP using both the PPG and ECG, into a student model, which predicts the BP using only PPG, while simultaneously training the two models. This knowledge distillation (KD) process is expected to improve the BP prediction performance of the student model.

5.2 Methods

A schematic of the proposed structure is presented in Fig. 5.1. The data preparation approach and convolutional neural network based prediction model reported in a previous work [1] were utilized, and the basic output transfer distillation method was used to realize the KD [26]. In contrast to the loss obtained by comparing the predicted and ground truth values of the model, the cross-entropy between the outputs of the teacher and student models was used as the loss:

$$L(n) = J(\sigma(\frac{f_t(x_n)}{T}), \sigma(\frac{f_s(x_n)}{T})) \tag{5.1}$$

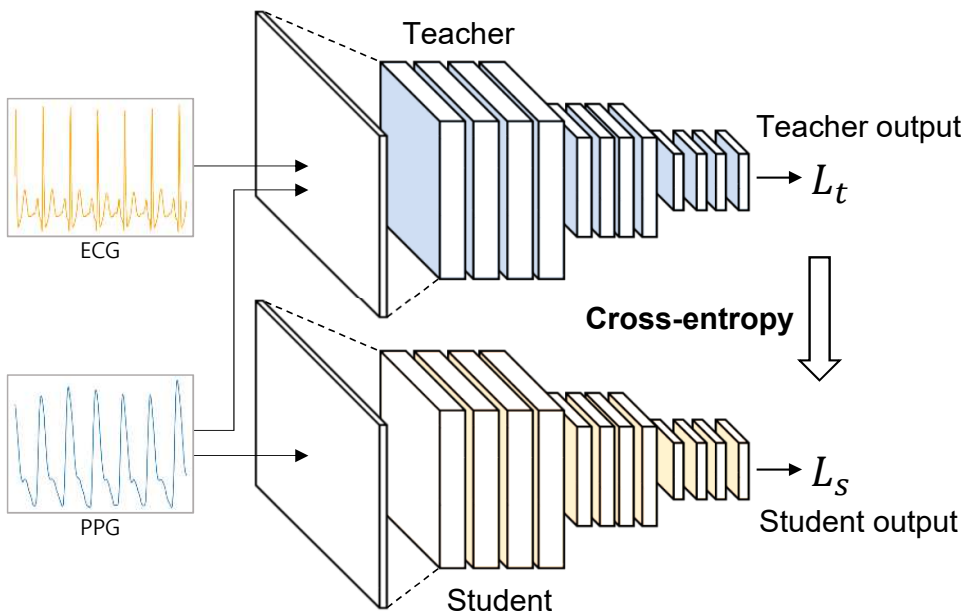

Figure 5.1: Schematic of BP prediction methodology.

5.3 Experimental results

Table 5.1 lists the BP prediction accuracies pertaining to the type of signal used for training and the utilization or lack thereof of KD. The teacher model is notably more accurate than the student model. However, when KD is employed, the BP prediction errors for systolic and diastolic BP are 10.27 and 5.33, respectively, which represent an improvement of 5.4% and 10.4% compared to the accuracy obtained when using the PPG signal alone as an input, respectively.

Table 5.1: BP Prediction performance for different models

	SBP(mmHg)		DBP(mmHg)	
	MAE	STD	MAE	STD
model w/ PPG & ECG	9.30	8.85	5.12	5.52
model w/ PPG	10.86	9.54	5.95	5.60
model w/ PPG + KD	10.27	9.28	5.33	5.34

5.4 Discussion & Summary

The proposed method can improve the accuracy of BP prediction using only PPG by employing KD. Future research will focus on improving the BP prediction performance by using other types of KD known to perform better, such as feature and sample transfer.

Chapter 6

Conclusion

In this dissertation, we introduced the various issues that exist in the study of predicting blood pressure using deep learning and how to solve them. In this chapter, we will summarize each issue introduced above and the contributions proposed to solve these issues, and introduce the expected effects and future work to further develop research.

Chapter 3 introduced a study to predict blood pressure from publicly available ECG and PPG datasets through a blood pressure prediction model with extraction and concentration CNN architecture. We proposed a novel end-to-end method of predicting blood pressure using only raw signals with no hand-made features. Based on the architecture of CNN, our method has the flexibility to deal with input variations (PPG/ECG, Time/Frequency) and applicability to real-world situations. Also the proposed method achieved excellent performance in predicting both systolic and diastolic blood pressure using the MIMIC II dataset compared with other known approaches.

In Chapter 4, we confirmed the performance of the BP prediction model developed by applying the PPG-BP dataset measured directly to the CNN-based BP pre-

diction model developed using the public dataset. We proposed a novel end-to-end method of predicting BP using only a single PPG signal without manual feature extraction. We optimized BP prediction performance by testing various combinations of PPG signal wavelengths to maximize prediction accuracy. Our CNN-based approach achieved comparable results to other approaches that require a single PPG signal.

In Chapter 5, we propose the knowledge distillation method to improve the accuracy of predicting blood pressure by using only photoplethysmogram. Specifically, the proposed approach distills the training knowledge of the teacher model, which predicts the BP using both photo-plethysmogram and electrocardiogram, into a student model, which predicts the BP using only photoplethysmogram, while simultaneously training the two models. The accuracy of the model using only photoplethysmogram to predict the systolic and diastolic blood pressure was improved by 5.4% and 10.4%, respectively, compared to the accuracy before using the knowledge distillation process.

6.1 Future work

There are several possible continuities in our proposed study, and will continue to be explored in the future. First, the method proposed in this paper can be used for wearable devices. Various studies have been conducted to easily and accurately measure biomedical signals such as ECG and PPG using wearable devices such as smart watches and smart rings. From the point of view of wearable application, it is essential to calibrate the blood pressure prediction model to be optimized for the individual after acquiring data for several hours and situations for each individual. Research into precise calibration techniques that tailor BP prediction models trained using various people's data to fit individuals using private data is expected to increase in the future. Second, it is possible to improve the performance of the blood pressure prediction model by securing data with a wide range of blood pressure values. A person's blood pressure is usually concentrated in a normal range, and in the case of general blood pressure data, the distribution of data forms a normal distribution, and the distribution is uneven for all range. In this case, the blood pressure prediction model is trained toward increasing the performance for the majority even if the performance for the minority is lowered. In future studies, it is expected that the blood pressure prediction performance can be improved through the design of the model considering the data distribution of these input signals. Third, we think that the performance of the blood pressure prediction model can be improved by applying different kinds of knowledge distillation method. The proposed method can improve the accuracy of BP prediction using only PPG by employing the most basic output transfer knowledge distillation method. Future research will focus on improving the BP prediction performance by using other types of knowledge distillation method known to perform better, such as feature and sample transfer.

Bibliography

[1] Sanghyun Baek, Jiyong Jang, and Sungroh Yoon. End-to-end blood pressure prediction via fully convolutional networks. *IEEE Access*, 7:185458–185468, 2019.

[2] Shaojie Bai, J Zico Kolter, and Vladlen Koltun. An empirical evaluation of generic convolutional and recurrent networks for sequence modeling. *arXiv preprint arXiv:1803.01271*, 2018.

[3] Federico S Cattivelli and Harinath Garudadri. Noninvasive cuffless estimation of blood pressure from pulse arrival time and heart rate with adaptive calibration. In *2009 Sixth international workshop on wearable and implantable body sensor networks*, pages 114–119. IEEE, 2009.

[4] Cheng-Chun Chang, Chien-Ta Wu, Byung Il Choi, and Tong-Jing Fang. Mw-ppg sensor: An on-chip spectrometer approach. *Sensors*, 19(17):3698, 2019.

[5] W Chen, T Kobayashi, S Ichikawa, Y Takeuchi, and T Togawa. Continuous estimation of systolic blood pressure using the pulse arrival time and intermittent calibration. *Medical and Biological Engineering and Computing*, 38(5):569–574, 2000.

[6] Yan Chen, Changyun Wen, Guocai Tao, and Min Bi. Continuous and noninva-

sive measurement of systolic and diastolic blood pressure by one mathematical model with the same model parameters and two separate pulse wave velocities. *Annals of biomedical engineering*, 40(4):871–882, 2012.

[7] Yu Cheng, Fei Wang, Ping Zhang, and Jianying Hu. Risk prediction with electronic health records: A deep learning approach. In *Proceedings of the 2016 SIAM International Conference on Data Mining*, pages 432–440. SIAM, 2016.

[8] Aram V Chobanian, George L Bakris, Henry R Black, William C Cushman, Lee A Green, Joseph L Izzo Jr, Daniel W Jones, Barry J Materson, Suzanne Oparil, Jackson T Wright Jr, et al. The seventh report of the joint national committee on prevention, detection, evaluation, and treatment of high blood pressure: the jnc 7 report. *Jama*, 289(19):2560–2571, 2003.

[9] Edward Choi, Mohammad Taha Bahadori, Andy Schuetz, Walter F Stewart, and Jimeng Sun. Doctor ai: Predicting clinical events via recurrent neural networks. In *Machine Learning for Healthcare Conference*, pages 301–318, 2016.

[10] Hyun-Soo Choi, Siwon Kim, Jung Eun Oh, Jee Eun Yoon, Jung Ah Park, Chang-Ho Yun, and Sungroh Yoon. Xgboost-based instantaneous drowsiness detection framework using multitaper spectral information of electroencephalography. In *Proceedings of the ACM International Conference on Bioinformatics, Computational Biology, and Health Informatics*, New York, NY, USA, 2018. ACM.

[11] Hyun-Soo Choi, Byunghan Lee, and Sungroh Yoon. Biometric authentication using noisy electrocardiograms acquired by mobile sensors. *IEEE Access*, 4:1266–1273, 2016.

[12] David. How to use a spygmomanometer.

[13] R Phillip Dellinger, Mitchell M Levy, Andrew Rhodes, Djillali Annane, Herwig Gerlach, Steven M Opal, Jonathan E Sevransky, Charles L Sprung, Ivor S Douglas, Roman Jaeschke, et al. Surviving sepsis campaign: international guidelines for management of severe sepsis and septic shock, 2012. *Intensive care medicine*, 39(2):165–228, 2013.

[14] Xiao-Rong Ding, Yuan-Ting Zhang, Jing Liu, Wen-Xuan Dai, and Hon Ki Tsang. Continuous cuffless blood pressure estimation using pulse transit time and photoplethysmogram intensity ratio. *IEEE Transactions on Biomedical Engineering*, 63(5):964–972, 2015.

[15] Xiaorong Ding, Bryan P Yan, Yuan-Ting Zhang, Jing Liu, Ni Zhao, and Hon Ki Tsang. Pulse transit time based continuous cuffless blood pressure estimation: A new extension and a comprehensive evaluation. *Scientific reports*, 7(1):11554, 2017.

[16] Gary M Drzewiecki, Julius Melbin, and Abraham Noordergraaf. Arterial tonometry: review and analysis. *Journal of biomechanics*, 16(2):141–152, 1983.

[17] Kefeng Duan, Zhiliang Qian, Mohamed Atef, and Guoxing Wang. A feature exploration methodology for learning based cuffless blood pressure measurement using photoplethysmography. In *2016 38th Annual International Conference of the IEEE Engineering in Medicine and Biology Society (EMBC)*, pages 6385–6388. IEEE, 2016.

[18] Vincent Dumoulin and Francesco Visin. A guide to convolution arithmetic for deep learning. *arXiv preprint arXiv:1603.07285*, 2016.

[19] Ömer Faruk Ertuğrul and Necmettin Sezgin. A noninvasive time-frequency-

based approach to estimate cuffless arterial blood pressure. *Turkish Journal of Electrical Engineering & Computer Sciences*, 26(5):2260–2274, 2018.

[20] Parry Fung, Guy Dumont, Craig Ries, Chris Mott, and Mark Ansermino. Continuous noninvasive blood pressure measurement by pulse transit time. In *The 26th annual international conference of the IEEE engineering in medicine and biology society*, volume 1, pages 738–741. IEEE, 2004.

[21] Heiko Gesche, Detlef Grosskurth, Gert Küchler, and Andreas Patzak. Continuous blood pressure measurement by using the pulse transit time: comparison to a cuff-based method. *European journal of applied physiology*, 112(1):309–315, 2012.

[22] Shrimanti Ghosh, Ankur Banerjee, Nilanjan Ray, Peter W Wood, Pierre Boulanger, and Raj Padwal. Using accelerometric and gyroscopic data to improve blood pressure prediction from pulse transit time using recurrent neural network. In *2018 IEEE International Conference on Acoustics, Speech and Signal Processing (ICASSP)*, pages 935–939. IEEE, 2018.

[23] Stephen K Glen, Henry L Elliott, Joan L Curzio, Kennedy R Lees, and John L Reid. White-coat hypertension as a cause of cardiovascular dysfunction. *The Lancet*, 348(9028):654–657, 1996.

[24] Arthur C Guyton, John Edward Hall, et al. *Textbook of medical physiology*, volume 548. Saunders Philadelphia, 1986.

[25] Rui He, Zhi-Pei Huang, Lian-Ying Ji, Jian-Kang Wu, Huihui Li, and Zhi-Qiang Zhang. Beat-to-beat ambulatory blood pressure estimation based on random forest. In *2016 IEEE 13th International Conference on Wearable and Implantable Body Sensor Networks (BSN)*, pages 194–198. IEEE, 2016.

[26] Geoffrey Hinton, Oriol Vinyals, and Jeff Dean. Distilling the knowledge in a neural network. *arXiv preprint arXiv:1503.02531*, 2015.

[27] Christian Holz and Edward J Wang. Glabella: Continuously sensing blood pressure behavior using an unobtrusive wearable device. *Proceedings of the ACM on Interactive, Mobile, Wearable and Ubiquitous Technologies*, 1(3):58, 2017.

[28] Toan Huu Huynh, Roozbeh Jafari, and Wan-Young Chung. Noninvasive cuffless blood pressure estimation using pulse transit time and impedance plethysmography. *IEEE Transactions on Biomedical Engineering*, 66(4):967–976, 2018.

[29] Monika Jain, Niranjan Kumar, Sujay Deb, and Angshul Majumdar. A sparse regression based approach for cuff-less blood pressure measurement. In *2016 IEEE International Conference on Acoustics, Speech and Signal Processing (ICASSP)*, pages 789–793. IEEE, 2016.

[30] Mohamad Kachuee, Mohammad Mahdi Kiani, Hoda Mohammadzade, and Mahdi Shabany. Cuff-less high-accuracy calibration-free blood pressure estimation using pulse transit time. In *2015 IEEE international symposium on circuits and systems (ISCAS)*, pages 1006–1009. IEEE, 2015.

[31] Mohammad Kachuee, Mohammad Mahdi Kiani, Hoda Mohammadzade, and Mahdi Shabany. Cuffless blood pressure estimation algorithms for continuous health-care monitoring. *IEEE Transactions on Biomedical Engineering*, 64(4):859–869, 2017.

[32] Akash P Kansagra, J Yu John-Paul, Arindam R Chatterjee, Leon Lenchik, Daniel S Chow, Adam B Prater, Jean Yeh, Ankur M Doshi, C Matthew Hawkins, Marta E Heilbrun, et al. Big data and the future of radiology informatics. *Academic radiology*, 23(1):30–42, 2016.

[33] Syed Ghufran Khalid, Jufen Zhang, Fei Chen, and Dingchang Zheng. Blood pressure estimation using photoplethysmography only: comparison between different machine learning approaches. *Journal of healthcare engineering*, 2018, 2018.

[34] Hui Kwon Kim, Seonwoo Min, Myungjae Song, Soobin Jung, Jae Woo Choi, Younggwang Kim, Sangeun Lee, Sungroh Yoon, and Hyongbum Henry Kim. Deep learning improves prediction of crispr–cpf1 guide rna activity. *Nature biotechnology*, 36(3):239, 2018.

[35] Ohhwan Kwon, Jinwoo Jeong, Hyung Bin Kim, In Ho Kwon, Song Yi Park, Ji Eun Kim, and Yuri Choi. Electrocardiogram sampling frequency range acceptable for heart rate variability analysis. *Healthcare informatics research*, 24(3):198–206, 2018.

[36] Yongbo Liang, Derek Abbott, Newton Howard, Kenneth Lim, Rabab Ward, and Mohamed Elgendi. How effective is pulse arrival time for evaluating blood pressure? challenges and recommendations from a study using the mimic database. *Journal of clinical medicine*, 8(3):337, 2019.

[37] Yongbo Liang, Zhencheng Chen, Rabab Ward, and Mohamed Elgendi. Hypertension assessment via ecg and ppg signals: An evaluation using mimic database. *Diagnostics*, 8(3):65, 2018.

[38] Yongbo Liang, Zhencheng Chen, Rabab Ward, and Mohamed Elgendi. Photoplethysmography and deep learning: Enhancing hypertension risk stratification. *Biosensors*, 8(4):101, 2018.

[39] Wan-Hua Lin, Hui Wang, Oluwarotimi Williams Samuel, Gengxing Liu, Zhen Huang, and Guanglin Li. New photoplethysmogram indicators for improving

cuffless and continuous blood pressure estimation accuracy. *Physiological measurement*, 39(2):025005, 2018.

[40] Jing Liu, Bryan P Yan, Yuan-Ting Zhang, Xiao-Rong Ding, Peng Su, and Ni Zhao. Multi-wavelength photoplethysmography enabling continuous blood pressure measurement with compact wearable electronics. *IEEE Transactions on Biomedical Engineering*, 66(6):1514–1525, 2018.

[41] National Heart Lung, Blood Institute, et al. Diseases and conditions index–hypotension. Technical report, Retrieved 2008-09-16, 2008.

[42] Wenjie Luo, Yujia Li, Raquel Urtasun, and Richard Zemel. Understanding the effective receptive field in deep convolutional neural networks. In *Advances in neural information processing systems*, pages 4898–4906, 2016.

[43] Plonsey Malmivuo, Jaakko Malmivuo, and Robert Plonsey. *Bioelectromagnetism: principles and applications of bioelectric and biomagnetic fields*. Oxford University Press, USA, 1995.

[44] Rikita Merai. Cdc grand rounds: a public health approach to detect and control hypertension. *MMWR. Morbidity and mortality weekly report*, 65, 2016.

[45] Fen Miao, Nan Fu, Yuan-Ting Zhang, Xiao-Rong Ding, Xi Hong, Qingyun He, and Ye Li. A novel continuous blood pressure estimation approach based on data mining techniques. *IEEE journal of biomedical and health informatics*, 21(6):1730–1740, 2017.

[46] Seonwoo Min, Byunghan Lee, and Sungroh Yoon. Deep learning in bioinformatics. *Briefings in bioinformatics*, 18(5):851–869, 2017.

[47] Riccardo Miotto, Fei Wang, Shuang Wang, Xiaoqian Jiang, and Joel T Dudley.

Deep learning for healthcare: review, opportunities and challenges. *Briefings in bioinformatics*, 2017.

[48] Seyedeh Somayyeh Mousavi, Mohammad Firouzmand, Mostafa Charmi, Mohammad Hemmati, Maryam Moghadam, and Yadollah Ghorbani. Blood pressure estimation from appropriate and inappropriate ppg signals using a whole-based method. *Biomedical Signal Processing and Control*, 47:196–206, 2019.

[49] J Muehlsteff, XL Aubert, and M Schuett. Cuffless estimation of systolic blood pressure for short effort bicycle tests: the prominent role of the pre-ejection period. In *2006 International Conference of the IEEE Engineering in Medicine and Biology Society*, pages 5088–5092. IEEE, 2006.

[50] Ramakrishna Mukkamala, Jin-Oh Hahn, Omer T Inan, Lalit K Mestha, Chang-Sei Kim, Hakan Töreyin, and Survi Kyal. Toward ubiquitous blood pressure monitoring via pulse transit time: theory and practice. *IEEE Transactions on Biomedical Engineering*, 62(8):1879–1901, 2015.

[51] Eoin O'brien, Bernard Waeber, Gianfranco Parati, Jan Staessen, and Martin G Myers. Blood pressure measuring devices: recommendations of the european society of hypertension. *Bmj*, 322(7285):531–536, 2001.

[52] Adam Paszke, Sam Gross, Soumith Chintala, Gregory Chanan, Edward Yang, Zachary DeVito, Zeming Lin, Alban Desmaison, Luca Antiga, and Adam Lerer. Automatic differentiation in pytorch. *in proc. NIPS AutodiffWorkshop*, 2017.

[53] Trang Pham, Truyen Tran, Dinh Phung, and Svetha Venkatesh. Deepcare: A deep dynamic memory model for predictive medicine. In *Pacific-Asia Conference on Knowledge Discovery and Data Mining*, pages 30–41. Springer, 2016.

[54] Thomas G Pickering, Kazuo Eguchi, and Kazuomi Kario. Masked hypertension: a review. *Hypertension Research*, 30(6):479, 2007.

[55] Thomas G Pickering, John E Hall, Lawrence J Appel, Bonita E Falkner, John Graves, Martha N Hill, Daniel W Jones, Theodore Kurtz, Sheldon G Sheps, and Edward J Roccella. Recommendations for blood pressure measurement in humans and experimental animals: part 1: blood pressure measurement in humans: a statement for professionals from the subcommittee of professional and public education of the american heart association council on high blood pressure research. *Hypertension*, 45(1):142–161, 2005.

[56] Artur Poliński, Krzysztof Czuszyński, and Tomasz Kocejko. Blood pressure estimation based on blood flow, ecg and respiratory signals using recurrent neural networks. In *2018 11th International Conference on Human System Interaction (HSI)*, pages 86–92. IEEE, 2018.

[57] CCY Poon and YT Zhang. Cuff-less and noninvasive measurements of arterial blood pressure by pulse transit time. In *2005 IEEE engineering in medicine and biology 27th annual conference*, pages 5877–5880. IEEE, 2006.

[58] Mustafa Radha, Koen De Groot, Nikita Rajani, Cybele CP Wong, Nadja Kobold, Valentina Vos, Pedro Fonseca, Nikolaos Mastellos, Petra A Wark, Nathalie Velthoven, et al. Estimating blood pressure trends and the nocturnal dip from photoplethysmography. *Physiological measurement*, 40(2):025006, 2019.

[59] Maynard Ramsey. Blood pressure monitoring: automated oscillometric devices. *Journal of clinical monitoring*, 7(1):56–67, 1991.

[60] Andrew Reisner, Phillip A Shaltis, Devin McCombie, and H Harry Asada. Util-

ity of the photoplethysmogram in circulatory monitoring. *Anesthesiology: The Journal of the American Society of Anesthesiologists*, 108(5):950–958, 2008.

[61] Mohammed Saeed, Mauricio Villarroel, Andrew T Reisner, Gari Clifford, Li-Wei Lehman, George Moody, Thomas Heldt, Tin H Kyaw, Benjamin Moody, and Roger G Mark. Multiparameter intelligent monitoring in intensive care ii (mimic-ii): a public-access intensive care unit database. *Critical care medicine*, 39(5):952, 2011.

[62] Manuja Sharma, Karinne Barbosa, Victor Ho, Devon Griggs, Tadesse Ghirmai, Sandeep Krishnan, Tzung Hsiai, Jung-Chih Chiao, and Hung Cao. Cuff-less and continuous blood pressure monitoring: a methodological review. *Technologies*, 5(2):21, 2017.

[63] S Shobitha, PM Amita, B Niranjana Krupa, and Gan Kok Beng. Cuffless blood pressure prediction from ppg using relevance vector machine. In *2017 International Conference on Electrical, Electronics, Communication, Computer, and Optimization Techniques (ICEECCOT)*, pages 75–78. IEEE, 2017.

[64] Josep Solà and Ricard Delgado-Gonzalo. *The Handbook of Cuffless Blood Pressure Monitoring: A Practical Guide for Clinicians, Researchers, and Engineers*. Springer Nature, 2019.

[65] Josep Maria Solà i Carós. *Continuous non-invasive blood pressure estimation*. PhD thesis, ETH Zurich, 2011.

[66] Peng Su, Xiao-Rong Ding, Yuan-Ting Zhang, Jing Liu, Fen Miao, and Ni Zhao. Long-term blood pressure prediction with deep recurrent neural networks. In *2018 IEEE EMBS International Conference on Biomedical & Health Informatics (BHI)*, pages 323–328. IEEE, 2018.

[67] Shaoxiong Sun, Rick Bezemer, X Long, J Muehlsteff, and RM Aarts. Systolic blood pressure estimation using ppg and ecg during physical exercise. *Physiological measurement*, 37(12):2154, 2016.

[68] Md Sayed Tanveer and Md Kamrul Hasan. Cuffless blood pressure estimation from electrocardiogram and photoplethysmogram using waveform based ann-lstm network. *Biomedical Signal Processing and Control*, 51:382–392, 2019.

[69] Charalambos Vlachopoulos, Michael O'Rourke, and Wilmer W Nichols. *McDonald's blood flow in arteries: theoretical, experimental and clinical principles*. CRC press, 2011.

[70] Ludi Wang, Wei Zhou, Ying Xing, and Xiaoguang Zhou. A novel neural network model for blood pressure estimation using photoplethesmography without electrocardiogram. *Journal of healthcare engineering*, 2018, 2018.

[71] Paul K Whelton, Robert M Carey, Wilbert S Aronow, Donald E Casey, Karen J Collins, Cheryl Dennison Himmelfarb, Sondra M DePalma, Samuel Gidding, Kenneth A Jamerson, Daniel W Jones, et al. 2017 acc/aha/aapa/abc/acpm/ags/apha/ash/aspc/nma/pcna guideline for the prevention, detection, evaluation, and management of high blood pressure in adults: a report of the american college of cardiology/american heart association task force on clinical practice guidelines. *Journal of the American College of Cardiology*, 71(19):e127–e248, 2018.

[72] Mico Yee-Man Wong, Carmen Chung-Yan Poon, and Yuan-Ting Zhang. An evaluation of the cuffless blood pressure estimation based on pulse transit time technique: a half year study on normotensive subjects. *Cardiovascular Engineering*, 9(1):32–38, 2009.

[73] Dan Wu, Lin Xu, Ruiqin Zhang, Heye Zhang, Lijie Ren, and Yuan-Ting Zhang. Continuous cuff-less blood pressure estimation based on combined information using deep learning approach. *Journal of Medical Imaging and Health Informatics*, 8(6):1290–1299, 2018.

[74] Xiaoman Xing and Mingshan Sun. Optical blood pressure estimation with photoplethysmography and fft-based neural networks. *Biomedical optics express*, 7(8):3007–3020, 2016.

[75] Liangwen Yan, Sijung Hu, Abdullah Alzahrani, Samah Alharbi, and Panagiotis Blanos. A multi-wavelength opto-electronic patch sensor to effectively detect physiological changes against human skin types. *Biosensors*, 7(2):22, 2017.

[76] Sung Sug Yoon, Cheryl D Fryar, and Margaret D Carroll. *Hypertension prevalence and control among adults: United States, 2011-2014*. US Department of Health and Human Services, Centers for Disease Control and Prevention, National Center for Health Statistics, 2015.

[77] Christopher C Young, Jonathan B Mark, William White, Ashley DeBree, Jeffery S Vender, and Andrew Fleming. Clinical evaluation of continuous noninvasive blood pressure monitoring: accuracy and tracking capabilities. *Journal of clinical monitoring*, 11(4):245–252, 1995.

[78] Yue Zhang and Zhimeng Feng. A svm method for continuous blood pressure estimation from a ppg signal. In *Proceedings of the 9th International Conference on Machine Learning and Computing*, pages 128–132. ACM, 2017.

[79] Liqiang Zheng, Zhaoqing Sun, Jue Li, Rui Zhang, Xingang Zhang, Shuangshuang Liu, Jiajin Li, Changlu Xu, Dayi Hu, and Yingxian Sun. Pulse pressure and mean arterial pressure in relation to ischemic stroke among patients with

uncontrolled hypertension in rural areas of china. *Stroke*, 39(7):1932–1937, 2008.

[80] Jian Zhou and Olga G Troyanskaya. Predicting effects of noncoding variants with deep learning–based sequence model. *Nature methods*, 12(10):931–934, 2015.

초 록

코로나 19에 의한 전 세계의 사회적 프로필 변화로, 규제와 신뢰성이 낮기 때문에 활성화 되지 않은 원격 의료 분야도 큰 변화를 겪을 것으로 예상됩니다. 코로나 19가 미국에 퍼짐에 따라 미국 보건복지부는 원격 진료의 표준을 일시적으로 완화하면서 페이스북, 페이스북 메신저 기반 화상 채팅, 행아웃, 스카이프를 사용한 원격 진료를 가능하게 했습니다. 원격의료 시장의 확장은 기존의 치료중심 병원 주도의 의료시장을 웨어러블, 빅 데이터 및 건강기록 분석을 통한 예방 및 관리에 중점을 둔 디지털 의료 서비스 시장으로 빠르게 변화시킬 것으로 예상됩니다. 이러한 예방 및 관리 중심의 디지털 헬스케어 서비스에서는 사람의 건강 상태를 쉽게 모니터링 할 수 있는 기술 개발이 매우 중요한데 혈압은 개인 건강 모니터링에 사용될 수 있는 필수 징후 중 하나 입니다.

고혈압은 아주 흔하고 위험한 질환입니다. 미국 성인 3명중 1명(약 7,500만명)이 고혈압을 가지고 있습니다. 이는 미국인의 주요 사망 원인 중 두가지인 심장 질환과 뇌졸중의 위험을 증가 시킵니다. 고혈압은 신체에 경고 신호나 자각 증상이 없어 많은 사람들이 자신이 고혈압인 것을 인지하지 못하기 때문에 "사일런트 킬러"라 불리웁니다. 이러한 이유로 정기적으로 쉽고 편리하게 혈압을 확인할 수 있는 기술의 개발이 매우 중요합니다. 생체의학 데이터 분석 분야에서는 머신 러닝을 대량으로 수집된 생체의학 빅 데이터에 적용하는 다양한 연구가 효과적으로 이루어지고 있습니다. 그러나 빅 데이터 수준으로 다량의 혈압 관련 데이터를 수집하는 것은 많은 전문적인 인력들이 오랜시간을 필요로 하기 때문에 매우 어렵고 비용 또한 많이 필요합니다. 따라서 본 학위논문에서는 이러한 문제를 극복하기 위한 3단계 전략을 제안했습니다.

먼저 누구나 시용할 수 있도록 공개되어 있는 심전도, 광용적맥파 데이터셋을 이용, 순차적인 심전도, 광용적맥파 신호에서 혈압을 잘 예측하도록 고안된 추출

및 농축 작업을 반복하는 함성곱 신경망 구조를 제안했습니다. 두번째로 제안된 합성곱 신경망 모델을 개인에게서 측정한 광용적맥파 신호를 이용해 제안된 함성곱 신경망 모델의 성능을 평가했습니다. 세번째로 혈압예측 모델의 정확성을 높이기 위해 지식 증류법과 입력신호 전처리 방법을 제안했습니다. 이 논문에서 제안된 모든 혈압예측 방법은 합성곱 신경망을 기반으로 합니다. 혈압 예측에 필요한 특징들을 수동으로 추출해야 하는 다른 연구들과 다르게 특징을 자동으로 추출하는 딥러닝의 장점을 활용, 아무런 처리도 하지 않은 원래 그대로의 생체 신호에서 신호 자체의 고유한 특징을 반영할 수 있습니다.

주요어: 머신러닝, 딥러닝, 커프리스 혈압측정, 합성곱 신경망, 생체의학 신호 분석
학번: 2016-30209